ARTICLES
https://doi.org/10.1038/s41558-022-01355-z

nature climate change

Check for updates

South Asian agriculture increasingly dependent on meltwater and groundwater

A. F. Lutz[1,2]✉, W. W. Immerzeel[1], C. Siderius[3], R. R. Wijngaard[4], S. Nepal[5,6], A. B. Shrestha[5], P. Wester[5] and H. Biemans[7]

Irrigated agriculture in South Asia depends on meltwater, monsoon rains and groundwater. Climate change alters the hydrology and causes shifts in the timing, composition and magnitude of these sources of water supply. Simultaneously, socio-economic growth increases water demand. Here we use a high-resolution cryosphere–hydrology–crop model forced with an ensemble of climate and socio-economic projections to assess how the sources of irrigation water supply may shift during the twenty-first century. We find increases in the importance of meltwater and groundwater for irrigated agriculture. An earlier melt peak increases meltwater withdrawal at the onset of the cropping season in May and June in the Indus, whereas increasing peak irrigation water demand during July and August aggravates non-renewable groundwater pumping in the Indus and Ganges despite runoff increases. Increasing inter-annual variability in rainfall runoff increases the need for meltwater and groundwater to complement rainfall runoff during future dry years.

The river basins of the Indus, Ganges and Brahmaputra in South Asia are home to almost one billion people[1], feature the largest continuous irrigation scheme in the world[2] and are also known as the bread basket and rice bowl of Asia. Agricultural production in the region, which yields around 300 Mt per year of food crops, depends largely on water supplied by irrigation[3]. The basins have distinct climates, controlled by different interactions of the south Asian summer monsoon and westerly disturbances. The monsoon is dominant in the southeast and gets weaker towards the northwest, where westerly disturbances protrude more frequently. This variation leads to substantial differences in the basins' hydrology. The upper Indus basin has much larger volumes of water stored as ice and snow compared with the upper Ganges and Brahmaputra[4] and therefore also generates more glacier melt and snowmelt[5,6]. Moreover, the downstream plain of the Indus is much more arid than the lower Ganges and Brahmaputra, making this the globe's river basin with the strongest dependence on meltwater[7,8].

Cryospheric and groundwater reserves provide buffering capacity to match the timing of supply and demand[9]. In the Indus, meltwater contributes around 40% of the water withdrawn for irrigation annually, compared with 4% in the Ganges and close to 0% in the Brahmaputra during 1981–2010[10] (Fig. 1). For the Indus, this contribution is around 60% during the pre-monsoon season. This period is generally dry but coincides with the sowing period for major crops grown during the *kharif* season (June–October). South Asia faces shortages of surface water to irrigate crops and therefore groundwater is extensively used, in particular in the Indus and Ganges[11]. Overdraft of groundwater is common and it is estimated that the Indo–Gangetic groundwater aquifer is depleted[12,13] by 40 mm per year to 90 mm per year.

The region is known as a global climate change hotspot for three reasons. First, water supply is strongly dependent on inflows from the Hindu Kush, Karakoram and Himalayan mountain ranges, which are particularly susceptible to climate change as a consequence of elevation-dependent warming[14] and a reduction in water-buffering capacity of glaciers and perennial snow packs[7]. Second, the region strongly depends on the Asian summer monsoon, which is projected to change notably in timing and magnitude[15]. Third, water demand is high and increasing rapidly, but water availability per capita is low and likely to decrease[16], and the transboundary basins have high potential for hydropolitical tension[17].

Climate change affects water resources in the rivers' headwaters. Glaciers are retreating in most of High Mountain Asia and are projected to retreat substantially further, regardless of the climate change scenario[18–20]. At the river-basin scale, the continued glacier wastage leads to an initial increase in meltwater, which peaks sometime during the twenty-first century, depending on the local circumstances, before it starts to decline[21]. Snowmelt volumes are projected to decline throughout the twenty-first century in all three basins[22]. However, most precipitation projections indicate increasing precipitation amounts in most of High Mountain Asia, albeit with large uncertainty, implying stable or increasing overall water availability throughout the twenty-first century[6,23]. Nevertheless, seasonal shifts[22], larger inter-annual variability in precipitation and a more rainfall-dominated and therefore more erratic hydrological regime may increase the frequency and length of dry periods, when meltwater and groundwater play important roles as water supply buffers and modulators of discharge[24–26]. On the downstream plains, increases in water demand due to higher evapotranspiration are expected in a warming climate, and despite projections of overall precipitation increase, the more erratic rainfall patterns may lead to more and longer droughts[23]. Global-scale work suggests that future reductions in terrestrial water storage lead to increases in future droughts[27] and also that changes in the cryosphere imply that irrigation demand needs to be partly met by water from other sources than meltwater[28].

Future socio-economic change leads to rapidly increasing water demand in South Asian countries. According to the high end of the Shared Socioeconomic Pathways (SSPs), the populations may

[1]Department of Physical Geography, Faculty of Geosciences, Utrecht University, Utrecht, The Netherlands. [2]FutureWater, Wageningen, The Netherlands. [3]Uncharted Waters, Sydney, Australia. [4]Department of Atmospheric Sciences, Yonsei University, Seoul, South Korea. [5]International Centre for Integrated Mountain Development, Kathmandu, Nepal. [6]International Water Management Institute, Nepal Office, Kathmandu, Nepal. [7]Wageningen Environmental Research, Wageningen, The Netherlands. ✉e-mail: a.f.lutz@uu.nl

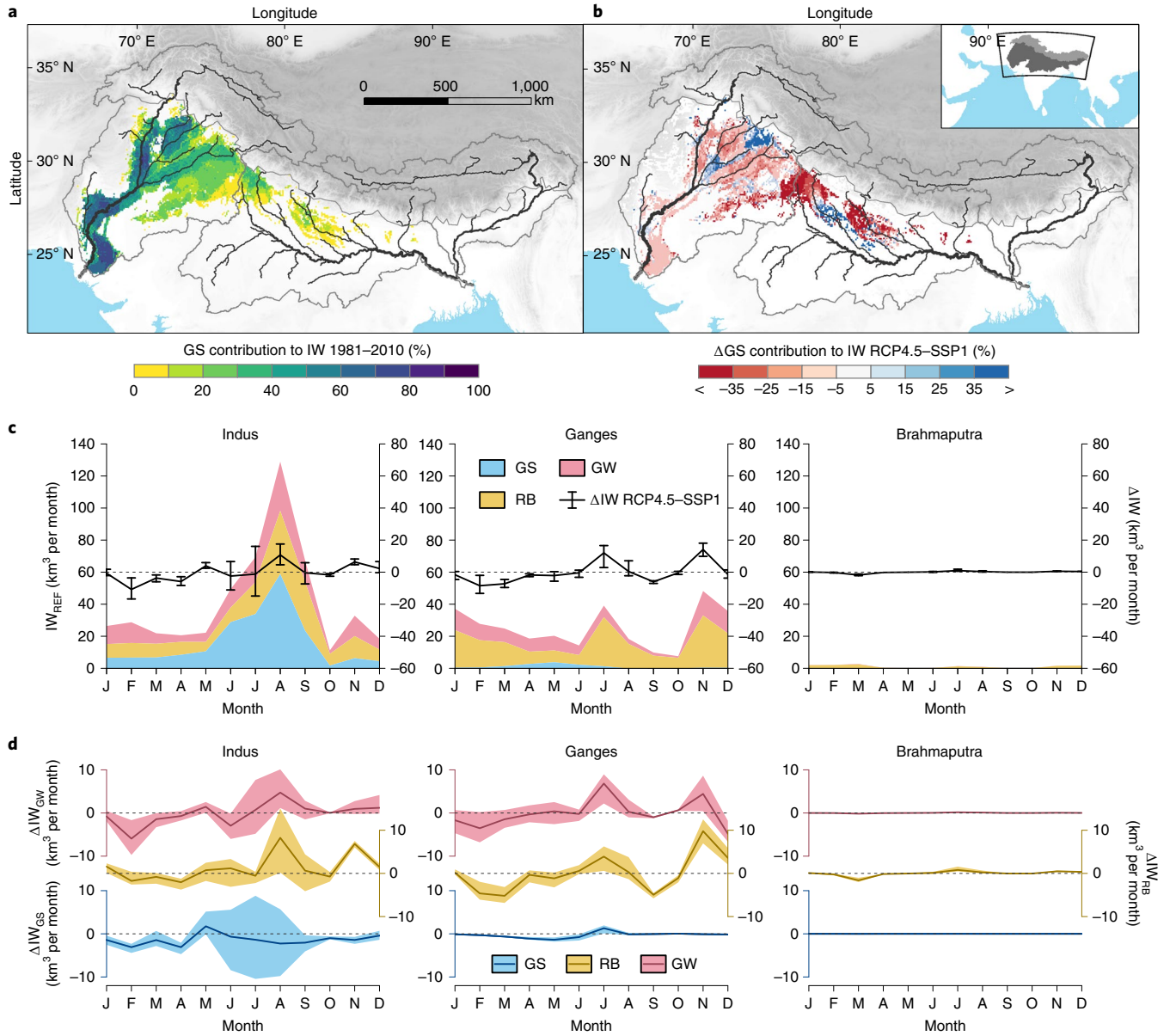

Fig. 1 | Historical irrigation withdrawals by source and projected future changes. a, Average contribution of glacier melt and snowmelt (GS) contribution to irrigation withdrawal (IW) during 1981–2010 (IW_{REF}). Grid cells with IW_{REF} < 10 mm per year are excluded. **b**, RCP4.5–SSP1 ensemble mean of projected changes in GS contribution (ΔGS) to irrigation withdrawal for 2071–2100 versus 1981–2010. **c**, Thirty-year average monthly irrigation withdrawals for the Indus, Ganges and Brahmaputra basins during 1981–2010, differentiated by source, including GS, rainfall runoff and baseflow (RB) and groundwater (GW). Black line indicates RCP4.5–SSP1 ensemble mean of projected change in average monthly total irrigation withdrawal (ΔIW) for 2071–2100 versus 1981–2010. Error bars indicate the ensemble spread in projections. Months are identified by first letter. **d**, Average monthly projected changes in irrigation withdrawal per source (groundwater, ΔIW_{GW}, pink; glacier melt and snowmelt, ΔIW_{GS}, blue; and rainfall runoff and baseflow, ΔIW_{RB}, yellow) for 2071–2100 versus 1981–2010. Lines and shading indicate the ensemble mean and ensemble range for RCP4.5–SSP1. Upstream and downstream river-basin boundaries (light grey tones) and main rivers (dark grey tones) are indicated in panels **a** and **b**. Background digital elevation model (GTOPO30) from ref. [45]. River data from ref. [46].

double (Ganges, Brahmaputra) or even triple (Indus) during the twenty-first century, whereas the lower end of the scenarios projects small growth in the Indus (13%) and decrease in the Ganges and Brahmaputra (7% and 12% decrease, respectively)[29]. Projections for cropland area range from 10% to 35% expansion[30]. Combined with economic growth and increases in standards of living, this will probably result in a vast growth in demand for water and food[31].

A key outstanding question therefore is how this growth in irrigation water demand can be reconciled with the climate change-induced hydrological changes. Here we integrate future changes in climate and socio-economic development and their impacts on upstream and downstream water resources by forcing a coupled high-resolution cryosphere–hydrology–crop model with an ensemble of downscaled climate scenarios and linked socio-economic pathways (Methods). We use this approach to quantify how the sources of irrigation withdrawals may shift in the future for three major South Asian river basins with contrasting climates and (changing) hydrological regimes.

Future shifts in water availability and irrigation demand

Downscaled climate change scenarios show basin-averaged projected temperature change in the three river basins ranging from

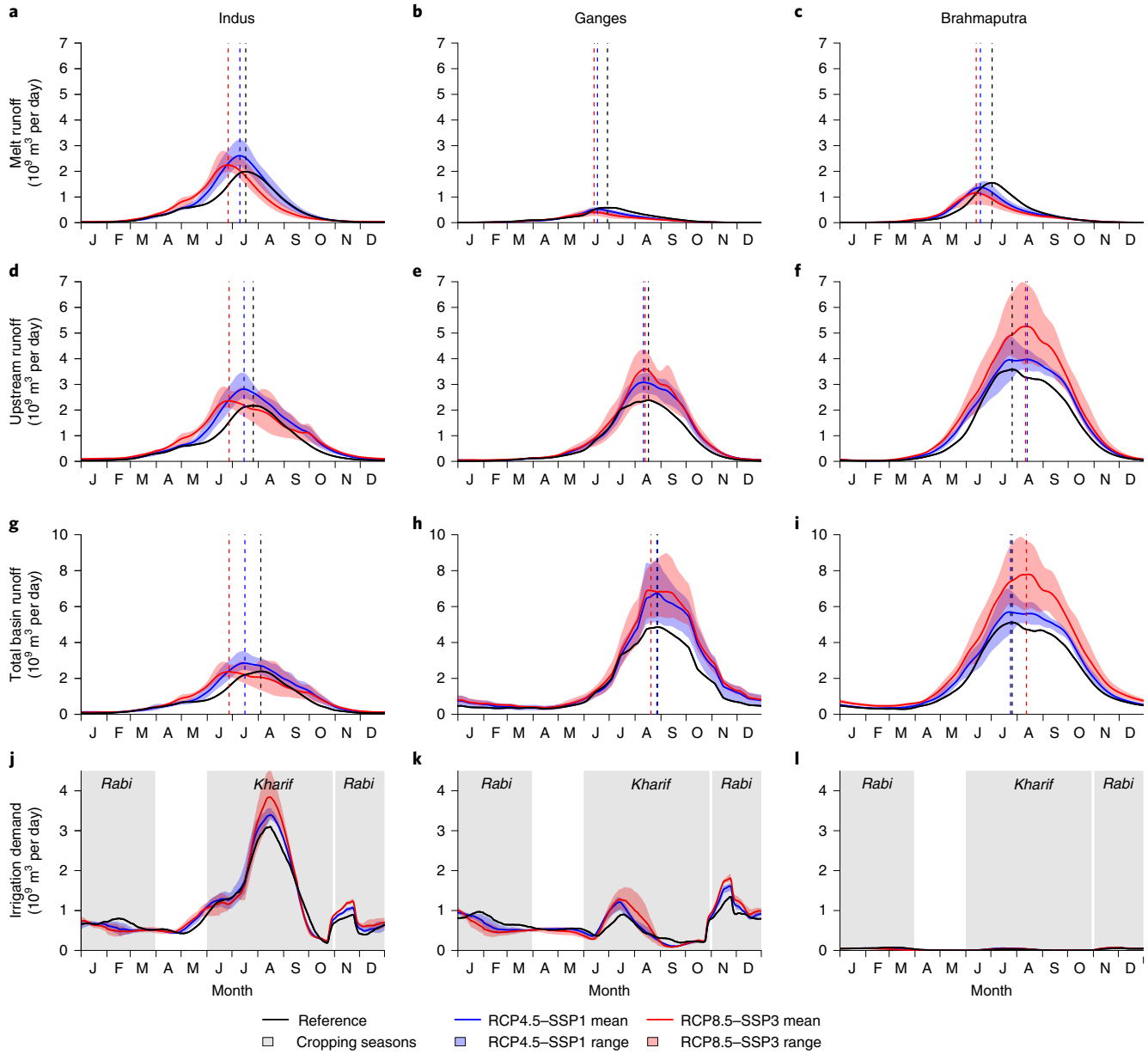

Fig. 2 | Future shifts in runoff and irrigation demand. a–c, Glacier melt and snowmelt runoff generated in the upstream basins of the Indus, Ganges and Brahmaputra. **d–f** Total runoff generated in the upstream basins. **g–i** Total summed runoff generated in the upstream and downstream basins. **j–l** The irrigation demand in the downstream basins. The plotted values are the ten day moving average of 30-year daily averages for the reference period (1981–2010, black solid line) and the end-of-century period (2071–2100). The blue solid line indicates the ensemble mean of the model runs forced with the RCP4.5–SSP1 combinations, and the blue shading indicates the ensemble range. The red solid line and red shading indicate the same for the RCP8.5–SSP3 combinations. Vertical dashed lines indicate the timing of the annual peak in runoff (maximum of ten day moving average) for 1981–2010 (black); 2071–2100 RCP4.5–SSP1 ensemble mean (blue); 2071–2100 RCP8.5–SSP3 ensemble mean (red). The grey shading in panels **j–l** indicates the region's major cropping seasons, *kharif* and *rabi*.

+1.1 to +5.6 °C and −9 to +35% for precipitation during 1981–2010 and 2071–2100, depending on the climate change scenario (Supplementary Table 1), with considerable intra-annual and spatial variability[23]. As a consequence, the hydrological response also varies and is the combined effect of future glacier change, shifts in snow and glacier melt onset and timing of their peaks, the transition towards a larger share of rainfall in precipitation and changes in precipitation sums and patterns. Comparing 2071–2100 with 1981–2010, the upper Indus shows an earlier onset of the high-flow season by one to two months, mainly caused by an earlier melt peak (Fig. 2a,d). In addition, the seasonal peak flow increases in magnitude for most scenarios due to a higher melt peak. In the Ganges, the earlier onset is not observed, because the meltwater contribution is smaller than in the Indus and has decreased by the end of the century compared with the reference period (Fig. 2b,e). The peak onset is mainly influenced by the monsoon. An increase in the seasonal peak flow is, however, projected for most scenarios both in Representative Concentration Pathway (RCP) 4.5 and RCP8.5 (Fig. 2e), due to a stronger monsoon. This increase in the seasonal flow peak is even more evident for the upper Brahmaputra, where in addition to the increase, the peak occurs about a month later in the year for the RCP8.5 ensemble mean compared with the reference

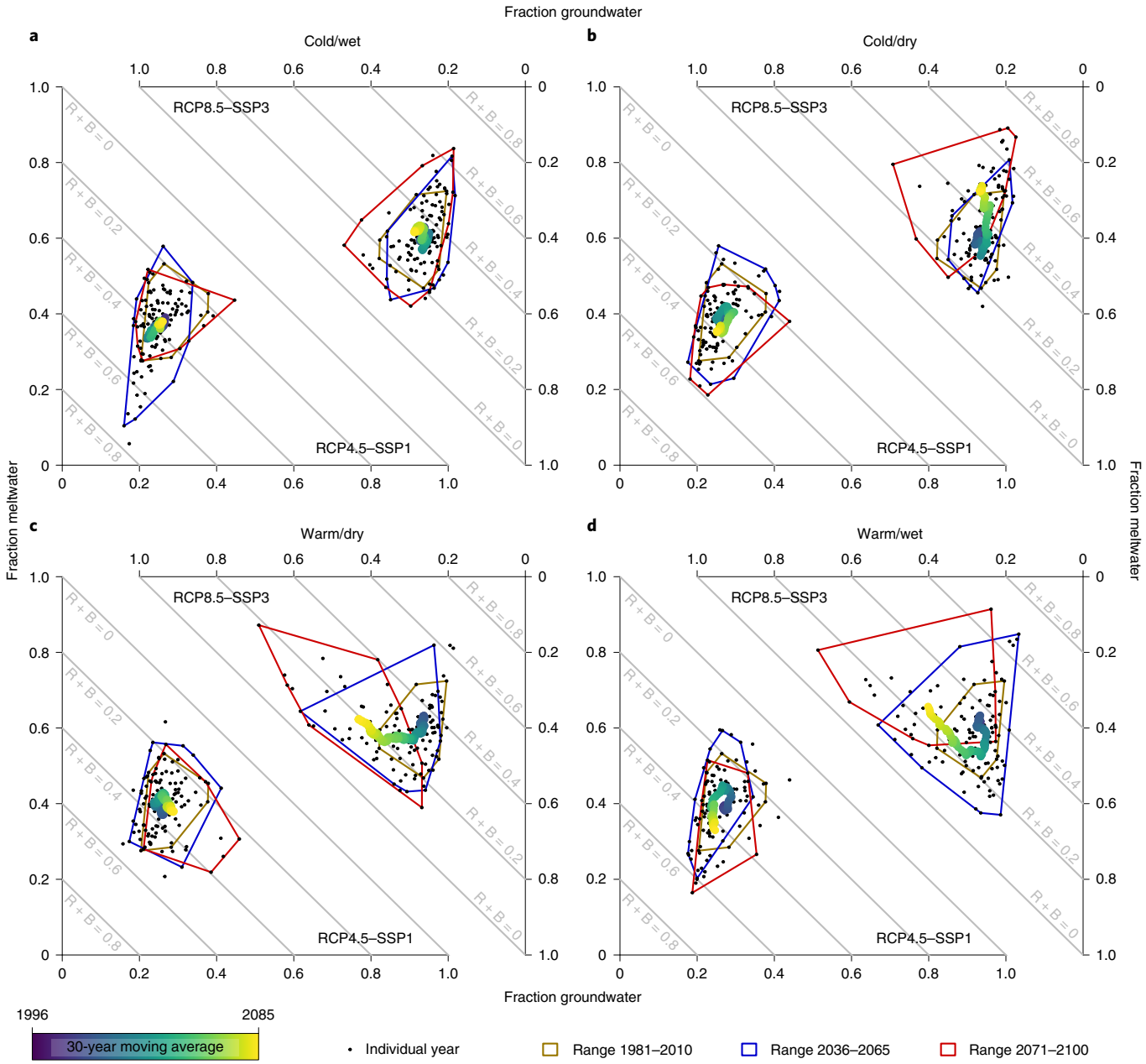

Fig. 3 | Shifting composition of irrigation withdrawals in the Indus basin. a–d, Dots indicate annual fractional basin-averaged contribution to irrigation withdrawal from groundwater (*x* axis), meltwater (*y* axis) and rainfall and baseflow (R + B, indicated by grey lines) for inidvidual years 1981–2100. Convex hulls indicate the range of years 1981–2010, 2036–2065 and 2071–2100. The colour scale shows the 30-year moving average starting at 1981–2010 and ending at 2071–2100. Separate plots are shown for cold/wet (**a**), cold/dry (**b**), warm/dry (**c**) and warm/wet (**d**) future scenarios. In each panel, results are shown for RCP4.5–SSP1 (lower left part of panel) and RCP8.5–SSP3 (upper right part of panel with flipped axis direction).

period (Fig. 2f). Strikingly, the onset of the high-flow season moves forward about one month for all climate scenarios here, which is related to increases in precipitation during the pre-monsoon season in the majority of downscaled general circulation models (GCMs) in our ensemble[32].

Increases in precipitation projected for most scenarios are also reflected in simulated changes in the runoff generation in the entire Ganges and Brahmaputra, in particular for the RCP8.5 ensemble members (Fig. 2h,i). The Brahmaputra shows a similar earlier onset of the high-flow season as its upstream basin. The Indus, however, does not show increases of the same order of magnitude, but a general shift in timing consistent with the seasonal shift in the upstream basin is clear (Fig. 2g).

The changes in future irrigation water demand show distinct patterns as well (Extended Data Fig. 1b,c and Fig. 2j–l). In the Indus and Ganges basins, most scenarios project slight overall increases in demand caused by an expansion of irrigated areas and higher crop evaporation demands in a warmer climate[33]. The demand increase is strongest for the RCP8.5–SSP3 ensemble members. In the Indus and Ganges, demand increases strongly during the onset of the *rabi* cropping season (November, 14% to 42% increase in the Indus and 13% to 43% increase in the Ganges for RCP4.5–SSP1 and RCP8.5–SSP3 ensemble members combined) (Fig. 2j,k). In both basins the demand also increases for most ensemble members during the middle of the *kharif* cropping season (July–August) and for the onset of the *kharif* season (May) in the Indus (12% to 41% increase for

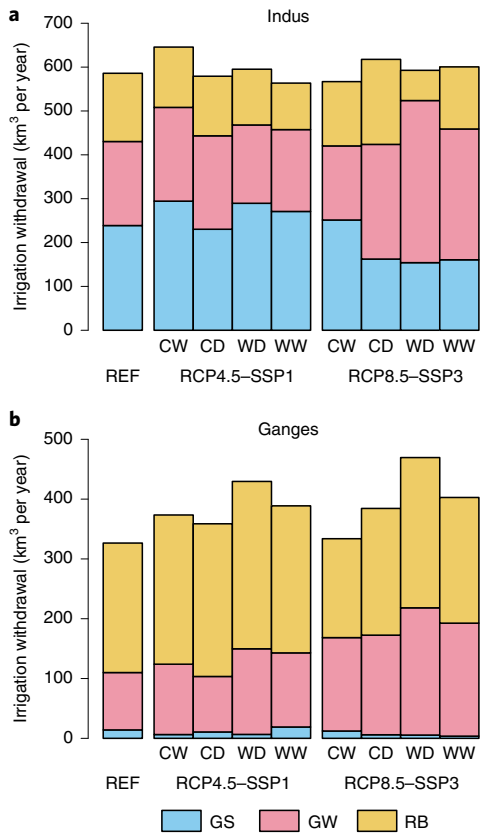

Fig. 4 | Composition of irrigation withdrawals during years with highest irrigation demand. a,**b**, Bar plots show annual irrigation withdrawal in the Indus basin (**a**) and Ganges basin (**b**) separated by source (GS, GW and RB) for the year with highest irrigation withdrawals during the reference period (1981–2010, REF) and the end of the century (2071–2100) for four ensemble members in the RCP4.5–SSP1 and RCP8.5–SSP3 scenarios, cold/wet (CW), cold/dry (CD), warm/dry (WD) and warm/wet (WW).

RCP4.5–SSP1 and 23–58% increase for RCP8.5–SSP3). In contrast, the demand decreases for most ensemble members in the second half of the *rabi* season (February–March, 6% to 37% decrease in the Indus and 9% to 34% decrease in the Ganges for RCP4.5–SSP1 and RCP8.5–SSP3 ensemble members combined) and the *kharif* season (September–October, 9% decrease to 11% increase in the Indus and 7% to 34% decrease in the Ganges for RCP4.5–SSP1 and RCP8.5–SSP3 ensemble members combined) in both basins as a result of shorter cropping seasons due to warming[33].

Combining these shifts, we conclude that a projected increase in runoff during the high-flow season as a result of enhanced melt (Indus) or a stronger monsoon (Ganges, Brahmaputra) coincides with an increase in irrigation water demand during the middle of the *kharif* season. Second, the earlier onset of the melt season in the Indus coincides with increasing irrigation water demand at the onset of the *kharif* season. Third, the attenuation of the hydrograph, with increasing flows during the low-flow season coincides with the increasing irrigation water demand at the onset of the *rabi* season. This indicates that climate change-induced shifts in water availability may help to support future increases in irrigation demands in the region.

Shifts in the sources of water for irrigation

Shifts in the timing of water supply and demand will result in a changing composition of irrigation water supply. In the Indus basin, meltwater becomes available earlier in the year at the end of the pre-monsoon season (May) when irrigation water demand increases as well. As a result, meltwater probably will play a more important role in the future during this critical moment in the agricultural year, with projections ranging from 0.1 km³ per month decrease to 6.4 km³ per month increase (Fig. 1d and Extended Data Fig. 2d). On the other hand, at the peak of the *kharif* season, when irrigation water demand is largest and increases the most compared with other periods of the year, the increase in withdrawals originates mainly from groundwater followed by surface water originating from rainfall and baseflow. In the RCP8.5–SSP3 ensemble, this increase in monthly irrigation water demand can be up to 55 km³ and needs to be met by an increase in groundwater withdrawals. The strongest increases in meltwater dependence are around the Chenab and Ravi tributaries (Fig. 1b, and Extended Data Fig. 2b). In RCP4.5–SSP1, an increase in surface water withdrawals originating from rainfall and baseflow leads to a reduction in groundwater withdrawals in much of Punjab and limits increases in groundwater withdrawals along the Indus main branch (Extended Data Fig. 3c,d). However, for the RCP8.5–SSP3 ensemble, groundwater withdrawals increase almost in the entire irrigated area of the Indus basin (Extended Data Fig. 3e).

In the Ganges basin, meltwater supply will have declined by the end of the century by about 9% (RCP4.5–SSP1 ensemble mean) to 29% (RCP8.5–SSP3 ensemble mean) at the annual scale (Fig. 2b), and this is reflected in the withdrawals for irrigation. For RCP4.5–SSP1 only, withdrawals from meltwater increase slightly during July, when the peak irrigation demand of the *kharif* season occurs (Fig. 1d). This increase is confined to the upstream region drawing water from the Ganges main branch (Fig. 1b). For RCP8.5–SSP3 meltwater availability has declined further than for the RCP4.5–SSP1 ensemble, and therefore meltwater plays a minimal role in irrigation withdrawals and declines basin-wide (Extended Data Fig. 2b,d). About half of the increases in the peak demands of the *kharif* season in July and *rabi* season in November can be met by withdrawals of surface water originating from rainfall and baseflow. The other half has to be met by groundwater withdrawals, which, similar as for the Indus, increase in almost the entire basin for the RCP8.5–SSP3 scenarios (Fig. 1d, Extended Data Fig. 2d and Extended Data Fig. 3e).

Strikingly, water withdrawals for irrigation decrease for the first half of the year in the Indus (except for May, the onset of the *kharif* season) and Ganges for most members in both the RCP4.5–SSP1 and RCP8.5–SSP3 ensembles (Fig. 1c and Extended Data Fig. 2c). This is related to the projected increases in rainfall lowering irrigation water demand during this period (Fig. 2j,k).

The shifts in the composition of irrigation water withdrawals throughout the twenty-first century are nonlinear. For example, for the warm/wet scenario in the RCP8.5–SSP3 ensemble, irrigation water composition in the Indus basin first shifts towards an increasing meltwater fraction and a lower rainfall runoff and baseflow fraction (Fig. 3d). Subsequently it shifts towards a lower meltwater fraction and higher groundwater fraction whereas the rainfall runoff and baseflow fraction remains fairly constant. These patterns differ per scenario and reflect intertwined processes of season-specific changes in climate resulting in changing melt patterns and shifts from snowfall to rainfall. For the month of May in the pre-monsoon season, increasing irrigation water withdrawals originating from meltwater are projected in the Indus (Fig. 1d and Extended Data Fig. 2d). This gradual shift in May towards a different irrigation water composition contrasts the annual trend (Fig. 3 and Extended Data Fig. 4). For example, for the warm/wet scenario in the RCP8.5–SSP3 ensemble, the composition in May first shifts towards a slightly lower meltwater contribution, which is then followed by a shift towards a higher meltwater contribution towards the end of the century.

The inter-annual variability in composition of irrigation water withdrawals is large and increases throughout the twenty-first century for most of the scenarios (Fig. 3, Extended Data Fig. 4 and

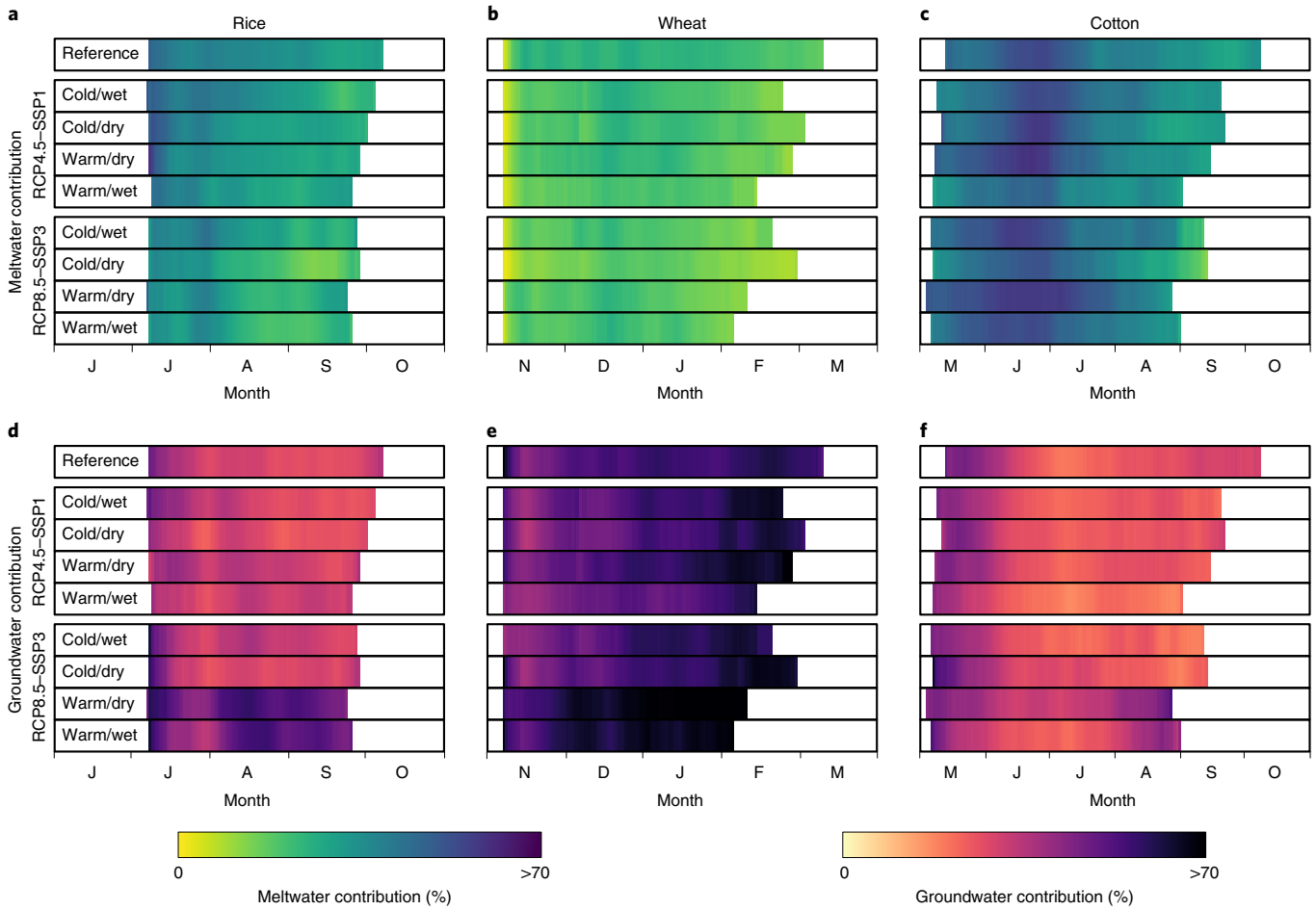

Fig. 5 | Contribution of meltwater and groundwater to irrigation for key crop types in the Indus river basin. a–c, The 30-year daily mean contribution of meltwater to irrigation withdrawal during the reference period (1981–2010) and end-of-century period (2071–2010) for each ensemble member in the RCP4.5–SSP1 and RCP8.5–SSP3 ensembles for rice (**a**), wheat (**b**) and cotton (**c**). **d–f**, The 30-year daily mean contribution of groundwater to irrigation withdrawal during 1981–2010 and 2071–2010 for each ensemble member for rice (**d**), wheat (**e**) and cotton (**f**). Months are identified by first letter, starting with June in **a** and **d**, November in **b** and **e** and May in **c** and **f**.

Extended Data Fig. 5). In the future, both meltwater and groundwater will gain importance in supplementing rainfall runoff as a source for irrigation water during drought years[23,34]. Withdrawals increase in all scenarios in the Ganges basin during these dry years (Fig. 4b) and have to be met mainly by increased groundwater withdrawals in all scenarios. The contributions of glacier melt and snowmelt decrease in all scenarios, simply because their availability has decreased. In contrast, in the Indus basin, where meltwater generation continues to increase towards the end of the century for RCP4.5–SSP1, withdrawals originating from meltwater increase substantially for almost all scenarios during extreme years (Fig. 4a). For most RCP8.5–SSP3 scenarios, the available meltwater declines towards the end of the century and a strong increase in groundwater dependence during years with high irrigation demand is apparent.

Key crops

Rice and wheat are the most commonly cultivated crops in the region[10]. The strongest increases in irrigation demand are projected for the *kharif* season (Fig. 2j,k), when rice is the major crop grown in both the Indus and Ganges (Fig. 5 and Extended Data Fig. 6), and the increasing demand during the *kharif* season can therefore largely be attributed to rice cultivation (Fig. 6c,d). This drives increases in groundwater withdrawals, in particular in the warm scenarios in RCP8.5–SSP3 (Fig. 5d and Extended Data Fig. 6d). In the RCP4.5–SSP1 scenarios, the relative meltwater contribution to irrigation withdrawals for rice increases at the onset of the *kharif* season in most ensemble members in both basins, resulting from the earlier onset of melt. This relative increase is however not visible for the RCP8.5–SSP3 ensemble members because the higher demand for irrigation water compared with RCP4.5–SSP1 drives additional groundwater pumping (Fig. 5a,d and Extended Data Fig. 6a,d).

The increase in meltwater availability during the pre-monsoon season in the Indus is also reflected in the meltwater contribution to withdrawals for irrigation of cotton in most scenarios (Fig. 5c). This is in contrast to wheat grown during the *rabi* season, when meltwater availability does not increase. Here groundwater will become even more important, in particular towards the end of the cropping season in February (Fig. 5b,e).

Interestingly, total irrigation water withdrawal in the Indus increases for rice but decreases for wheat, cotton and sugarcane for the RCP4.5–SSP1 and RCP8.5–SSP3 ensemble means in both basins (Fig. 6c,d). The shortening of the cropping season due to increased temperatures which influence crop phenology is much more pronounced for the latter-mentioned crops than for rice.

Non-renewable groundwater abstractions

In our modelling approach, irrigation water supply that cannot be met by withdrawals of surface water is assumed to be met by

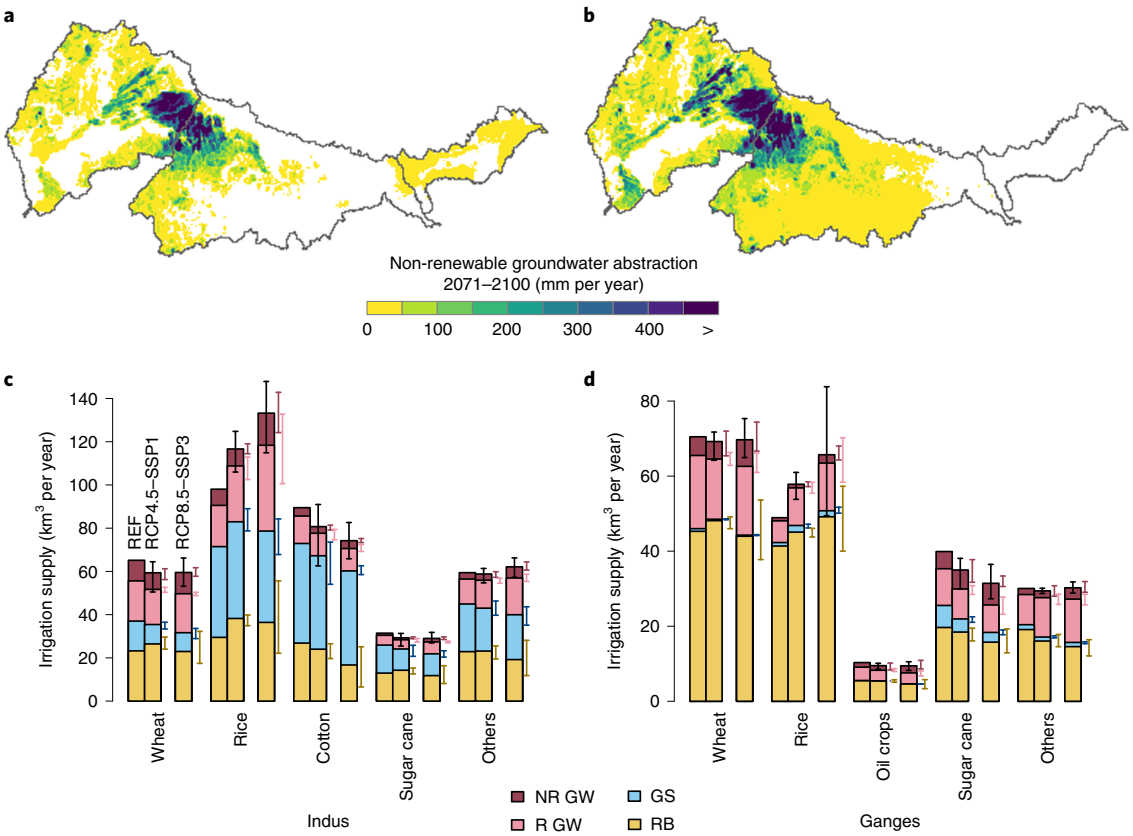

Fig. 6 | Non-renewable groundwater abstraction. a,**b**, The non-renewable groundwater abstraction in the Indus, Ganges and Brahmaputra river basins for the end of the century (2071–2100) for the RCP4.5–SSP1 (**a**) and RCP8.5–SSP3 (**b**) ensemble means. **c**,**d**, The irrigation supply by source (non-renewable groundwater (NR GW), renewable groundwater (R GW), glacier melt and snowmelt (GS) and rainfall runoff and baseflow (RB)) for major crops in the Indus (**c**) and Ganges (**d**) river basins during the reference period (1981–2010, REF) and ensemble means for 2071–2100 (RCP4.5–SSP1 and RCP8.5–SSP3). Error bars at the bar tops indicate the ensemble range of projections for total irrigation supply. Error bars to the right of the bars indicate the ensemble range of projections of each contributor to irrigation supply.

groundwater withdrawals (Methods). We distinguish renewable and non-renewable groundwater withdrawals in our projections for the future (Fig. 6). Increases in irrigation water demand for rice cultivation in the Indus and Ganges basin are the main drivers of the increase in groundwater demand (Fig. 6c,d). Hotspots for future groundwater depletion are projected in the Punjab region and further downstream in the Indus in Pakistan's Sindh province (Fig. 6a,b). These regions already face adverse effects of groundwater depletion under the current climate and socio-economic situation[35]. Strikingly, these regions are also the hotspots for decreasing contribution of meltwater to irrigation withdrawals, implying that reduced availability of meltwater will aggravate groundwater depletion here (Fig. 1b and Extended Data Fig. 2b). At the basin scale, we project increasing meltwater availability towards the end of the century in the Indus basin (Fig. 2a), which dampens the increase in pressure on groundwater sources in this basin but does not reduce it (Fig. 6). And even in this basin with its extraordinary large ice reserves, meltwater generation will decline eventually[21], putting further stress on groundwater resources, similar as projected for the Ganges basin in this study.

Adaptation

The mounting pressure on meltwater and groundwater sources resulting from climate change and socio-economic growth requires targeted adaptation strategies targeting water-use efficiency and water availability. Increases in melt runoff, primarily in the Indus basin, partially buffer higher demand in the initial decades, providing a window of opportunity to adapt to declining buffering capacity in the longer term. There is still potential to improve regional agricultural water productivity, although the financial feasibility of water conservation measures in a region with low farm-level profitability remains a matter of concern[36], and the effect on water consumption at the basin scale may remain limited[37]. Given the strong and increasing dependence on meltwater and groundwater at the onset of the *kharif* season during the pre-monsoon season for rice and cotton in the Indus and rice in the Ganges basin, a change in crop type or shift in sowing date to later in the year can provide potential solutions[38], in particular when cropping cycles get shorter in a warmer climate. The Hindu Kush, Karakoram and Himalayan mountain ranges have a large untapped hydropower potential[39], which is rapidly being deployed. The environmentally sustainable management[40] of multi-purpose reservoirs could increase the region's water-buffering capacity and relieve pressure on meltwater and groundwater sources, while at the same time reducing the long-lasting regional electricity deficits[41]. Such interventions can only be successful provided that they are governed from a river-basin perspective considering upstream–downstream linkages, highlighting the need for transboundary cooperation[42], inclusive and conjunctive water use and consideration of trade-offs and synergies between the water–energy–food-nexus components in these basins[43,44].

Online content

Any methods, additional references, Nature Research reporting summaries, source data, extended data, supplementary information, acknowledgements, peer review information; details of

author contributions and competing interests; and statements of data and code availability are available at https://doi.org/10.1038/s41558-022-01355-z.

Received: 5 August 2021; Accepted: 28 March 2022;
Published online: 19 May 2022

References

1. Wester, P., Mishra, A., Mukherji, A. & Bhakta Shrestha, A. (eds) *The Hindu Kush Himalaya Assessment: Mountains, Climate Change, Sustainability and People* (Springer, 2019).
2. Jain, S. K., Agarwal, P. K. & Singh, V. P. in *Hydrology and Water Resources of India* (eds Jain, S.K. et al.) 473–511 (Springer, 2007).
3. Biemans, H., Siderius, C., Mishra, A. & Ahmad, B. Crop-specific seasonal estimates of irrigation-water demand in South Asia. *Hydrol. Earth Syst. Sci.* **20**, 1971–1982 (2016).
4. Farinotti, D. et al. A consensus estimate for the ice thickness distribution of all glaciers on Earth. *Nat. Geosci.* **12**, 168–173 (2019).
5. Lutz, A. F., Immerzeel, W. W., Shrestha, A. B. & Bierkens, M. F. P. Consistent increase in High Asia's runoff due to increasing glacier melt and precipitation. *Nat. Clim. Change* **4**, 587–592 (2014).
6. Khanal, S. et al. Variable 21st century climate change response for rivers in High Mountain Asia at seasonal to decadal time scales. *Water Resour. Res.* https://doi.org/10.1029/2020WR029266 (2021).
7. Immerzeel, W. W. et al. Importance and vulnerability of the world' s water towers. *Nature* **577**, 364–369 (2019).
8. Viviroli, D., Kummu, M., Meybeck, M., Kallio, M. & Wada, Y. Increasing dependence of lowland populations on mountain water resources. *Nat. Sustain.* **3**, 917–928 (2020).
9. Nie, Y. et al. Glacial change and hydrological implications in the Himalaya and Karakoram. *Nat. Rev. Earth Environ.* https://doi.org/10.1038/s43017-020-00124-w (2021).
10. Biemans, H. et al. Importance of snow and glacier meltwater for agriculture on the Indo-Gangetic Plain. *Nat. Sustain.* **2**, 594–601 (2019).
11. Gleeson, T., Wada, Y., Bierkens, M. F. P. & van Beek, L. P. H. Water balance of global aquifers revealed by groundwater footprint. *Nature* **488**, 197–200 (2012).
12. Döll, P., Schmied, H. M., Shuh, C., Portmann, F. T. & Eicker, A. Global-scale assessment of groundwater depletion and related groundwater abstractions: combining hydrological modeling with information from well observations and GRACE satellites. *Water Resour. Res.* **50**, 5698–5720 (2014).
13. Rodell, M., Velicogna, I. & Famiglietti, J. S. Satellite-based estimates of groundwater depletion in India. *Nature* **460**, 999–1002 (2009).
14. Pepin, N. et al. Elevation-dependent warming in mountain regions of the world. *Nat. Clim. Change* **5**, 424–430 (2015).
15. Turner, A. G. & Annamalai, H. Climate change and the South Asian summer monsoon. *Nat. Clim. Change* **2**, 587–595 (2012).
16. Kirby, M., Mainuddin, M., Khaliq, T. & Cheema, M. Agricultural production, water use and food availability in Pakistan: historical trends, and projections to 2050. *Agric. Water* **179**, 34–46 (2016).
17. De Stefano, L., Petersen-Perlman, J. D., Sproles, E. A., Eynard, J. & Wolf, A. T. Assessment of transboundary river basins for potential hydro-political tensions. *Glob. Environ. Change* **45**, 35–46 (2017).
18. Kraaijenbrink, P. D. A., Bierkens, M. F. P., Lutz, A. F. & Immerzeel, W. W. Impact of a global temperature rise of 1.5 degrees Celsius on Asia's glaciers. *Nature* https://doi.org/10.1038/nature23878 (2017).
19. Rounce, D. R., Hock, R. & Shean, D. E. Glacier mass change in High Mountain Asia through 2100 using the open-source Python Glacier Evolution Model (PyGEM). *Front. Earth Sci.* https://doi.org/10.3389/feart.2019.00331 (2020).
20. Hugonnet, R. et al. Accelerated global glacier mass loss in the early twenty-first century. *Nature* **592**, 726–731 (2021).
21. Huss, M. & Hock, R. Global-scale hydrological response to future glacier mass loss. *Nat. Clim. Change* https://doi.org/10.1038/s41558-017-0049-x (2018).
22. Kraaijenbrink, P. D. A., Stigter, E. E., Yao, T. & Immerzeel, W. W. Climate change decisive for Asia's snow meltwater supply. *Nat. Clim. Change* https://doi.org/10.1038/s41558-021-01074-x (2021).
23. Lutz, A. F. et al. South Asian river basins in a 1.5 °C warmer world. *Reg. Environ. Change* **19**, 833–847 (2019).
24. Pritchard, H. D. Asia's shrinking glaciers protect large populations from drought stress. *Nature* **569**, 649–654 (2019).
25. Wijngaard, R. R. et al. Future changes in hydro-climatogical extremes in the upper Indus, Ganges, and Brahmaputra river basins. *PLoS ONE* **12**, e0190224 (2017).
26. Van Tiel, M., Van Loon, A., Seibert, J. & Stahl, K. Hydrological response to warm and dry weather: do glaciers compensate? *Hydrol. Earth Syst. Sci. Discuss.* https://doi.org/10.5194/hess-2021-44 (2021).
27. Pokhrel, Y. et al. Global terrestrial water storage and drought severity under climate change. *Nat. Clim. Change* **11**, 226–233 (2021).
28. Qin, Y. et al. Agricultural risks from changing snowmelt. *Nat. Clim. Change* **10**, 459–465 (2020).
29. KC, S. & Lutz, W. The human core of the shared socioeconomic pathways: population scenarios by age, sex and level of education for all countries to 2100. *Glob. Environ. Change* **42**, 181–192 (2017).
30. Popp, A. et al. Land-use futures in the shared socio-economic pathways. *Glob. Environ. Change* **42**, 331–345 (2017).
31. Munia, H. A. et al. Future transboundary water stress and its drivers under climate change: a global study. *Earth's Future* **8**, e2019EF001321 (2020).
32. Lutz, A. F., Maat, W., Biemans, H. & Shrestha, A. B. Selecting representative climate models for climate change impact studies: an advanced envelope-based selection approach. *Int. J. Climatol.* https://doi.org/10.1002/joc.4608 (2016).
33. Wijngaard, R. R. et al. Climate change vs. socio-economic development: understanding the South-Asian water gap. *Hydrol. Earth Syst. Sci.* **22**, 6297–6321 (2018).
34. Wen, S. et al. Population exposed to drought under the 1.5 °C and 2.0 °C warming in the Indus River basin. *Atmos. Res.* **218**, 296–305 (2019).
35. Cheema, M. J. M., Immerzeel, W. W. & Bastiaanssen, W. G. M. Spatial quantification of groundwater abstraction in the irrigated indus basin. *Groundwater* **52**, 25–36 (2014).
36. Siderius, C. et al. Financial feasibility of water conservation in agriculture. *Earth's Future* **9**, e2020EF001726 (2021).
37. Grafton, R. Q. et al. The paradox of irrigation efficiency. *Science* **361**, 748–750 (2018).
38. Shah, H., Siderius, C. & Hellegers, P. Limitations to adjusting growing periods in different agroecological zones of Pakistan. *Agric. Syst.* **192**, 103184 (2021).
39. Gernaat, D. E. H. J., Bogaart, P. W., van Vuuren, D. P., Biemans, H. & Niessink, R. High-resolution assessment of global technical and economic hydropower potential. *Nat. Energy* https://doi.org/10.1038/s41560-017-0006-y (2017).
40. Grill, G. et al. Mapping the world's free-flowing rivers. *Nature* **569**, 215–221 (2019).
41. Molden, D. J., Vaidya, R. A., Shrestha, A. B., Rasul, G. & Shrestha, M. S. Water infrastructure for the Hindu Kush Himalayas. *Int. J. Water Resour. Dev.* **30**, 60–77 (2014).
42. Vinca, A. et al. Transboundary cooperation a potential route to sustainable development in the Indus basin. *Nat. Sustain.* **4**, 331–339 (2021).
43. Rasul, G., Neupane, N., Hussain, A. & Pasakhala, B. Beyond hydropower: towards an integrated solution for water, energy and food security in South Asia. *Int. J. Water Resour. Dev.* **37**, 466–490 (2021).
44. Wu, X., Jeuland, M., Sadoff, C. & Whittington, D. Interdependence in water resource development in the Ganges: an economic analysis. *Water Policy* **15**, 89–108 (2013).
45. Gesch, D. B., Verdin, K. L. & Greenlee, S. K. New land surface digital elevation model covers the Earth. *Eos Trans. AGU* **80**, 69–70 (2019).
46. Lehner, B. & Grill, G. Global river hydrography and network routing: baseline data and new approaches to study the world's large river systems. *Hydrol. Process.* **27**, 2171–2186 (2013).

Methods

Hydrological models. We coupled two hydrological models which have been jointly applied to the Indus, Ganges and Brahmaputra basins in earlier work to assess the future development of the South Asian water gap[33] and the historical contribution of meltwater to South Asian agriculture[10]. The upstream model domain includes all high mountain ranges in the river basins and ends at the transition of the mountains to the plains where the first major reservoirs are located (Supplementary Fig. 1). For the upstream model domain, we use the spatially distributed cryospheric–hydrological Spatial Processes in Hydrology (SPHY) model[47] at 5×5 km with a daily time step. This model has been specifically developed for applications at the river-basin scale under data scarcity. The daily total runoff generated in each grid cell is calculated, being the sum of glacier melt and snowmelt runoff, rainfall runoff (that is, the sum of surface runoff and lateral flow) and baseflow. The total runoff and its components are subsequently routed downstream, using a routing scheme that uses a digital elevation model and a recession coefficient to obtain daily discharge for each grid cell. To estimate the contribution of snowmelt and glacier melt to runoff, sub-grid variability at 100×100 m resolution is taken into account. A fractional ice cover ranging between 0 (no ice cover) and 1 (complete ice cover) is calculated at the sub-grid level and assigned to each 5×5 km model grid cell. For each complete or partial glacier within a 5×5 km model grid cell, information of the glacier mean elevation, initial ice thickness and the type of glacier (that is, debris-free or debris-covered) is added. The type of glacier is determined based on thresholds for slope and elevation[48]. Initial ice thicknesses are estimated with the GlabTop2 methodology[49]. Glacier melt is calculated using a degree–day approach[50], where different melt factors are assigned to debris-free and debris-covered glaciers. Part of the meltwater subsequently becomes surface runoff, and the remainder becomes baseflow, where this distinction is determined by a calibrated glacier-runoff fraction. Changes in the fractional glacier cover in response to changes in temperature and precipitation are included using a mass-conserving algorithm for ice redistribution.

Snow accumulation is determined for each grid cell with a daily precipitation and temperature threshold to distinguish between rain and snow. Snowmelt is simulated using a degree–day approach[50], and sublimation is estimated with an elevation-dependent potential sublimation function[51]. The snow module includes refreezing and water storage in the snowpack. Snowmelt runoff is generated when the liquid storage in the snowpack exceeds the threshold. The liquid and dry snow storage is updated daily after summing/subtracting all incoming and outgoing fluxes. Rainfall runoff is calculated according to the saturation excess runoff principle. For the root zone layer, the modified Hargreaves reference evapotranspiration equation[52] and crop coefficient depending on land use are implemented to calculate the actual evapotranspiration. Lateral flow of water in the soil between grid cells and vertical exchange of water between soil layers through percolation and capillary rise are accounted for. Each grid cell has a groundwater reservoir, and depending on the amount of simulated recharge from the sub-soil layer, releases delayed baseflow to the runoff. The runoff and its composition is routed downstream to the outlets of 27 catchments comprising the upstream model domain (Supplementary Fig. 1). At these outlets the runoff feeds into the downstream hydrology–crop model. Further details of the SPHY model are described in ref. [47], and more details about this specific setup are described in ref. [25].

For the downstream model domain (Supplementary Fig. 1), we use the Lund–Potsdam–Jena managed land model (LPJmL), which simulates the daily water balance, crop growth and irrigation water demand at a 5×5 minute grid scale at a daily time step. In LPJmL coupled hydrology and carbon cycles are simulated, and therefore the model is suitable to analayse the interactions between water availability and crop growth and production[53]. LPJmL simulates the daily water balance at the sub-grid scale. Water is added to a grid cell through precipitation or irrigation, and part of it becomes direct surface runoff while another part infiltrates into the soil. Subsequently, five soil layers of variable thickness are included through which the infiltrated water percolates. A part flows to the river system as subsurface runoff when soil water content exceeds saturation. Water can also leave the soil by evaporation from the upper soil layer or through transpiration by natural vegetation or crops[54]. Runoff that enters the river system flows through this system at a constant flow velocity of 1 m s^{-1} (ref. [55]). The effect of large reservoirs on streamflow and water supply for irrigation is simulated by a generic reservoir-operation scheme that is applied for all reservoirs in the study area included in the Global Reservoir and Dam (GRanD) database[56] (Supplementary Fig. 1). The reservoir-operation scheme regulates the release of water from reservoirs as a function of reservoir characteristics, downstream irrigation demand in the area that can be supplied and a minimum release to sustain environmental flow requirements. Reservoir characteristics include storage capacity, the primary purpose of the reservoir (for example, irrigation, hydropower, flood control, navigation), actual storage and reservoir elevation to estimate which irrigated areas can be supplied from the reservoir. The reservoir-operation scheme is described in detail in ref. [57]. This generic scheme is used because detailed data on the operation of individual reservoirs is not publicly available. The setup used in this study simulates a double cropping system, including monsoon-season crops (*kharif*) and winter-season crops (*rabi*)[3]. The daily irrigation demand for an irrigated crop in a cell is calculated as the minimum amount of water needed to be applied at the field to fill the soil to field capacity and the amount needed to fulfil the potential evapotranspiration. Subsequently, the withdrawal demand is calculated by adding losses during conveyance, distribution and application of water. Application losses depend on the type of irrigation system (surface, sprinkler or drip) and the soil type[58]. We refer to the water withdrawn to fulfil this demand as 'irrigation withdrawal'. We assume that all irrigated cropland in the Indus, Ganges and Brahmaputra basins is sustained by surface irrigation systems in the reference period and the future scenarios. The consumed irrigation water (blue water consumption of irrigation) is defined as evapotranspiration of irrigation water that is supplied to the field. The irrigation module is described in detail in section 2.6.2 of ref. [58]. The consumed fractions we find (Supplementary Table 2) are in agreement with other studies in the region[59]. We keep CO_2 concentrations constant in model simulations of the future because of the large uncertainty regarding CO_2 effects on irrigation water demand in the future[60], and the response of the LPJmL model with constant CO_2 concentrations falls in the middle of the uncertainty range projected by other hydrology and crop models[61]. The future role of CO_2 fertilization is still one of the factors leading to uncertainty in future irrigation demand projections.

The daily supply of water for non-agricultural uses and irrigation is dependent on the availability of water. Upstream grid cells get priority over downstream grid cells. At the grid-cell level, water for non-agricultural uses gets priority and is supplied first. Previous research with the LPJmL model shows that applying different priority schemes at the grid-cell level have only a limited effect[62], but effects can be large when different priorities are assigned at river-basin scale[63]. Subsequently, water for irrigation is supplied from surface water (that is, rivers, lakes and reservoirs) and distributed through an extensive irrigation canal system. The surface water destined for irrigation sometimes travels hundreds of kilometres through a vast network of larger (inter-sub-basin) and smaller canals before reaching the irrigated fields. We identified irrigation command areas based on maps of irrigation canals and connected them to command area inlets (locations at the main rivers where the water is diverted from the river into the canal system) to simulate this transport. The irrigated fields within the command areas can be supplied by surface water extracted from the main river at the command area inlet (Supplementary Fig. 1).

For this surface water, we distinguish by source as meltwater runoff, rainfall runoff and baseflow (that is, runoff that is slowly released from the groundwater reservoir of grid cells when it is saturated) before it is routed downstream as surface water. If irrigation demand cannot be fulfilled by the available surface water, water is withdrawn from groundwater. In our study this water is defined by its source as groundwater. A groundwater store in each cell is filled by daily groundwater recharge, which equals the water percolating through the lower soil layer. This groundwater can be extracted for irrigation if surface water is insufficiently available. Besides, the groundwater is contributing to surface water as baseflow, using a linear reservoir algorithm as in ref. [64]. When groundwater withdrawals in a grid cell exceed the recharge over a longer period of time, groundwater ceases to contribute to baseflow and withdrawals are unsustainable and lead to depletion as in ref. [65]. We define a net loss of groundwater being the difference between abstractions and recharge in a grid cell over multiple years as non-renewable groundwater abstractions. We assume unlimited groundwater availability for each grid cell, and lateral flow of groundwater is not represented in the model. Further details of this specific LPJmL setup are described in refs. [10,33].

Quantifying the sources of irrigation water withdrawals. To estimate the composition of irrigation water withdrawals, a series of model simulations were performed for each future scenario (eight scenarios in total; two RCP–SSP combinations with four climate scenarios each):

(1) A run where only surface water from baseflow and rainfall runoff can be used to fulfil irrigation and other demands.
(2) A run where all surface water, including snowmelt and glacier melt, can be used to fulfil irrigation and other demands.
(3) A run where irrigation and other demands are supplied from surface water and groundwater. For this run, we assume that groundwater is applied only when surface water is not sufficiently available. In this simulation groundwater supply is not restricted but indicates depletion when groundwater withdrawal is greater than groundwater recharge over longer time scales.

By comparing outputs of these runs, the individual contributions of rainfall runoff plus baseflow, meltwater and non-renewable and renewable groundwater to water supply can be estimated. We assume that the difference in water withdrawals between two subsequent runs can be completely attributed to the source added in the latter run. The total withdrawals are represented by run 3 output. The contribution of rainfall and baseflow to withdrawals is estimated with run 1 output. The contribution of meltwater to withdrawals is estimated as run 2 output minus run 1 output. The contribution of groundwater is estimated as run 3 output minus run 2 output.

Input data. *Reference climate.* LPJmL is forced with daily mean air temperature, precipitation and long and shortwave radiation. To bring the carbon pools in equilibrium, a 1,000-year spin-up run forced by the WATCH Forcing Data

methodology applied to ERA-Interim reanalysis (WFDEI)[66] dataset is used. For the reference and future runs, the model is forced with a reference climate dataset for the Indus, Ganges and Brahmaputra river basins[23]. SPHY is forced with daily precipitation, mean, maximum and minimum air temperature from the same reference climate dataset. This reference-forcing dataset is based on the WFDEI dataset but is downscaled to 5×5 km resolution for the upstream basins and 10×10 km for the downstream basins using high-resolution elevation data and temperature-lapse rates. For the upstream basins, an additional correction for the underestimation of high-altitude precipitation has been implemented using glacier mass-balance data as a proxy to improve actual precipitation amounts[67]. To run LPJmL, the dataset has been re-gridded to a 5 min resolution regular latitude-longitude grid.

Soil. The soil data for LPJmL was derived from the Harmonized World Soil Database[68], from which we used the 13 classes of the US Department of Agriculture texture classes. The original data were re-gridded to a 5 min resolution based on a majority rule. For the SPHY model, soil information is derived from HiHydroSoil[69], which is a high-resolution map of hydraulic properties derived from the Harmonized World Soil Database[68] using pedo-transfer functions.

Reference land use. For LPJmL, gridded fractions of 12 rain-fed and irrigated crops for the *kharif* and *rabi* seasons are derived from MIRCA2000[70] as in ref. [3] but kept at 5 min resolution. We have added cotton growing during the early *kharif* season, rather than as a perennial crop. Especially in the Indus basin, total irrigation water withdrawals for cotton form a large share of the total irrigation water withdrawal. Land use classes in the SPHY model are taken from GlobCover, resampled to 5×5 km resolution[71].

Sowing dates. Sowing dates are implemented as in ref. [3]. *Kharif* crops are assumed to be sown five days after the onset of the monsoon and therefore depend on the location. An exception is made for cotton, which is sown on 1 April in the whole region except for the Punjab region in Pakistan, where it is sown on 1 May[70]. *Rabi* crops are sown on 1 November in the whole region.

Reference domestic and industrial demand. Gridded domestic and industrial water demand and consumption datasets at 5×5 min resolution are taken from the PCRaster GLOBal Water Balance (PCR-GLOBWB) model and used in the downstream LPJmL model[72]. The demand data are based on population data[73], country-specific per capita domestic water-withdrawal data and water-use intensities[74]. Both industrial and domestic water demand is assumed to remain constant throughout the year. LPJmL is forced with consumption data so that return flows are included. Details are described in ref. [33].

Glaciers. Glacier outlines for the SPHY model are derived from the Randolph Glacier Inventory version 5.0 (ref. [75]) and are gridded to a 100×100 m grid. The glaciers are intersected with the 5×5 km model grid and for each glacier–model grid-cell combination, a unique ID, debris flag, elevation and initial ice thickness is assigned.

Drainage. The drainage direction of grid cells is derived from the HydroSheds global database[46] for both SPHY and LPJmL. For the downstream model (LPJmL), we used the 5 min version of the drainage-direction map (B. Lehner, personal communication).

Climate change scenarios. We use an ensemble of climate change scenarios for RCP4.5 and RCP8.5[76]. For each RCP we applied the empirical–statistical downscaling method of quantile mapping to four selected GCM runs to bias correct and downscale the GCM runs to the model resolutions of, respectively, SPHY (upstream) and LPJmL (downstream), as described in detail in ref. [23]. The GCM runs were selected to cover a wide envelope in the range of projections in the Coupled Model Intercomparison Project (CMIP) 5 multi-model ensemble and show sufficient skill in simulating the historical climate[32,77].

Socio-economic scenarios. We link the SSP scenarios[78], SSP1, following the 'sustainability' narrative, and SSP3, following the 'regional rivalry' narrative, to RCP4.5 and RCP8.5, respectively. Future domestic and industrial water-demand datasets are extracted from the IMAGE v3.0 model[79]. Within the IMAGE model, a sub-model is included[80] that calculates the future domestic and industrial water demands based on projections for population growth and economic development (based on gross domestic product per capita) that are consistent with the selected SSPs.

We also use the SSP1 and SSP3 regional-scale projections of IMAGE[81] to derive changes in rain-fed and irrigated cropland extents at the country scale. We assume that both the crop distribution and crop types in the future remain consistent with the reference period and impose the rates of change in area for irrigated and rain-fed crop lands from the IMAGE projections to our MIRCA2000-based reference land-use data. Details are described in the Data and Methods sections in ref. [33].

India's river-interlinking project plans the realization of transfers connecting tributaries within the Ganges basin and between the Ganges and Brahmaputra basins. These are all still in the planning stage, and we did not include them in the model.

Model calibration and validation. A two-step systematic approach was used to calibrate and validate the upstream model. First, model parameters related to glacier and snow processes were calibrated to MODIS remote sensing snow-cover[82] and geodetic glacier mass-balance data[83] over three upstream catchments (Supplementary Fig. 1). Second, the remaining model parameters, which are related to soil hydrological processes and routing, were calibrated to observed discharge at six gauging locations, two in each river basin (Supplementary Fig. 1 and Supplementary Tables 3 and 5). By using this two-step approach, problems related to equifinality, which are common in the simulation of high-mountain hydrology, could be minimized[84]. The model performance has been validated at the same locations for different time periods than the calibration. The approach and results are described in detail in ref. [25]. To validate the performance of the coupled SPHY–LPJmL model in simulating discharge, simulated and observed flows were compared at three downstream gauging locations near the outlets of the three river basins (Supplementary Fig. 1 and Supplementary Table 3). Locations near the basin outlets have been selected to cover effects of flow alterations through reservoir operations and water withdrawals. For most of the stations, the model performance is satisfactory to very good with Nash–Sutcliffe efficiencies[85] above 0.6 and up to 0.83, and biases below ±25% (ref. [86])(Supplementary Table 3). The location Kotri Barrage is an exception, where model performance is unsatisfactory, and also the 34% bias at Hardinge bridge is considerable. The poorer model performance at Kotri Barrage suggests that losses from the river (water diversion into canals, abstraction for irrigation, evaporation and infiltration) might be underestimated. River infiltration and evaporation can explain part of the difference. However, just upstream of Kotri Barrage, there are large irrigation canals diverting water from the river. In addition, the simulated irrigation water withdrawals in Pakistan are higher than most other estimates[3].

Simulated crop yields were calibrated to sub-national agricultural statistics for the years 2003–2008 (Supplementary Fig. 5 in ref. [10]). Three coupled parameters that represent management intensity (that is, maximum leaf-area index, maximum harvest index and a parameter to scale leaf-level biomass production to grid level) were calibrated. A sub-national calibration of crop yields allows for a representation of spatial heterogeneity in crop yields as a result of different management practices in addition to the variations caused by differences in climate. The sub-national calibration is described in more detail in ref. [3]. The difference in this study is that cotton is also included here. Furthermore, the *kharif* and *rabi* yields were merged into one single value for calibration. Caloric content of the different crops are taken from food composition tables as listed by the Food and Agriculture Organization of the United Nations[87].

Data availability

The data generated in this study (that is, outputs of model simulations) are available in an online archive at https://doi.org/10.24416/UU01-BY9O4S. Elevation data used in this study are available at https://www.hydrosheds.org. The reference climate data and downscaled climate change scenarios used in this study are available at https://rds.icimod.org/Home/Data?group=30. Glacier outlines used in this study are available at https://www.glims.org/RGI/. Snow-cover data used in this study are available at https://nsidc.org/data/modis/data_summaries#snow. Soil data used in this study are available at https://www.futurewater.eu/projects/hihydrosoil/. Land use data used in this study are available at http://due.esrin.esa.int/page_globcover.php and https://www.uni-frankfurt.de/45218031/Data_download_center_for_MIRCA2000. SSP data used in this study are available at https://tntcat.iiasa.ac.at/SspDb. Population data used in this study are available at https://dataportaal.pbl.nl/downloads/HYDE/HYDE3.2/. IMAGE v3.0 data used in this study are available at https://models.pbl.nl/image/index.php/Download.

Code availability

Code for the SPHY model is available at https://github.com/FutureWater/SPHY. Code for the LPJmL model is available at https://github.com/PIK-LPJmL/LPJmL.

References

47. Terink, W., Lutz, A. F., Simons, G. W. H., Immerzeel, W. W. & Droogers, P. SPHY v2.0: Spatial processes in HYdrology. *Geosci. Model Dev.* **8**, 2009–2034 (2015).
48. Paul, F., Huggel, C. & Kääb, A. Combining satellite multispectral image data and a digital elevation model for mapping debris-covered glaciers. *Remote Sens. Environ.* **89**, 510–518 (2004).
49. Frey, H. et al. Estimating the volume of glaciers in the Himalayan–Karakoram region using different methods. *Cryosphere* **8**, 2313–2333 (2014).
50. Hock, R. Temperature index melt modelling in mountain areas. *J. Hydrol.* **282**, 104–115 (2003).
51. Lutz, A. F., Immerzeel, W. W., Kraaijenbrink, P. D. A., Shrestha, A. B. & Bierkens, M. F. P. Climate change impacts on the upper Indus hydrology: sources, shifts and extremes. *PLoS ONE* **11**, e0165630 (2016).
52. Droogers, P. & Allen, R. G. Estimating reference evapotranspiration under inaccurate data conditions. *Irrig. Drain. Syst.* **16**, 33–45 (2002).
53. Gerten, D. et al. Global water availability and requirements for future food production. *J. Hydrometeorol.* **12**, 885–899 (2011).

54. Schaphoff, S. et al. Contribution of permafrost soils to the global carbon budget. *Environ. Res. Lett.* **8**, 014026 (2013).
55. Rost, S. et al. Agricultural green and blue water consumption and its influence on the global water system. *Water Resour. Res.* **44**, W09405 (2008).
56. Lehner, B. et al. *Global Reservoir and Dam Database, v.1 (GRanDv1): Reservoirs, Revision 01* (NASA Socioeconomic Data and Applications Center, 2011); https://sedac.ciesin.columbia.edu/data/set/grand-v1-dams-rev01
57. Biemans, H. et al. Impact of reservoirs on river discharge and irrigation water supply during the 20th century. *Water Resour. Res.* **47**, W03509 (2011).
58. Jägermeyr, J. et al. Water savings potentials of irrigation systems: global simulation of processes and linkages. *Hydrol. Earth Syst. Sci.* **19**, 3073–3091 (2015).
59. Simons, G. W. H., Droogers, P., Contreras, S., Sieber, J. & Bastiaanssen, W. G. M. A novel method to quantify consumed fractions and non-consumptive use of irrigation water: application to the Indus Basin Irrigation System of Pakistan. *Agric. Water Manag.* **236**, 106174 (2020).
60. Keenan, T. F. et al. A constraint on historic growth in global photosynthesis due to increasing CO_2. *Nature* **600**, 253–258 (2021).
61. Elliott, J. et al. Constraints and potentials of future irrigation water availability on agricultural production under climate change. *Proc. Natl Acad. Sci. USA* **111**, 3239–3244 (2014).
62. Bijl, D. L. et al. A global analysis of future water deficit based on different allocation mechanisms. *Water Resour. Res.* **54**, 5803–5824 (2018).
63. de Vos, L., Biemans, H., Doelman, J. C., Stehfest, E. & Van Vuuren, D. P. Trade-offs between water needs for food, utilities, and the environment—a nexus quantification at different scales. *Environ. Res. Lett.* **16**, 115003 (2021).
64. Alcamo, J. et al. Development and testing of the WaterGAP 2 global model of water use and availability. *Hydrol. Sci. J.* **48**, 317–337 (2003).
65. Wada, Y. et al. Global depletion of groundwater resources. *Geophys. Res. Lett.* **37**, L20402 (2010).
66. Weedon, G. P. et al. The WFDEI meteorological forcing data set: WATCH Forcing Data methodology applied to ERA-Interim reanalysis data. *Water Resour. Res.* https://doi.org/10.1002/2014WR015638 (2014).
67. Immerzeel, W. W., Wanders, N., Lutz, A. F., Shea, J. M. & Bierkens, M. F. P. Reconciling high altitude precipitation with glacier mass balances and runoff. *Hydrol. Earth Syst. Sci.* **12**, 4755–4784 (2015).
68. *Harmonized World Soil Database* (v.1.2) (FAO/IIASA/ISRIC/ISSCAS/JRC, 2012); https://www.fao.org/soils-portal/soil-survey/soil-maps-and-databases/harmonized-world-soil-database-v12/ru/
69. Boer, F. D. *HiHydroSoil: A High Resolution Soil Map of Hydraulic Properties* v.1.2 (FutureWater, 2016).
70. Portmann, F. T., Siebert, S. & Döll, P. MIRCA2000—Global monthly irrigated and rainfed crop areas around the year 2000: a new high-resolution data set for agricultural and hydrological modeling. *Glob. Biogeochem. Cycles* **24**, GB1011 (2010).
71. Defourny, P. et al. GLOBCOVER: A 300 m global land cover product for 2005 using ENVISAT MERIS time series. In *Proc. ISPRS Commission VII Mid-Term Symposium: Remote Sensing: From Pixels to Processes* (eds Kerle, N. & Skidmore, A.) (International Society of Photogrammetry and Remote Sensing, 2007).
72. Wada, Y., Wisser, D. & Bierkens, M. F. P. Global modeling of withdrawal, allocation and consumptive use of surface water and groundwater resources. *Earth Syst. Dyn.* **5**, 15–40 (2014).
73. Klein Goldewijk, K., Beusen, A., Van Drecht, G. & De Vos, M. The HYDE 3.1 spatially explicit database of human-induced global land-use change over the past 12,000 years. *Glob. Ecol. Biogeogr.* **20**, 73–86 (2011).
74. *AQUASTAT database* (FAO, 2016); https://www.fao.org/aquastat/en/
75. Arendt, A. et al. *Randolph Glacier Inventory [5.0]: A Dataset of Global Glacier Outlines,* v.5.0 (Global Land Ice Measurements from Space (GLIMS), 2015); https://www.glims.org/RGI/
76. van Vuuren, D. P. et al. A new scenario framework for climate change research: scenario matrix architecture. *Climatic Change* **122**, 373–386 (2014).
77. Taylor, K. E., Stouffer, R. J. & Meehl, G. A. An overview of CMIP5 and the experiment design. *Bull. Am. Meteorol. Soc.* **93**, 485–498 (2012).
78. O'Neill, B. C. et al. The roads ahead: narratives for Shared Socioeconomic Pathways describing world futures in the 21st century. *Glob. Environ. Change* **42**, 169–180 (2017).
79. Stehfest, E., et al. *Integrated Assessment of Global Environmental Change with IMAGE 3.0.—Model Description and Policy Applications* (Netherlands Environmental Assessment Agency, 2014).
80. Bijl, D. L., Bogaart, P. W., Kram, T., de Vries, B. J. M. & van Vuuren, D. P. Long-term water demand for electricity, industry and households. *Environ. Sci. Policy* **55**, 75–86 (2016).
81. Doelman, J. C. et al. Exploring SSP land-use dynamics using the IMAGE model: regional and gridded scenarios of land-use change and land-based climate change mitigation. *Glob. Environ. Change* **48**, 119–135 (2018).
82. Hall, D. K. & Riggs, G. A. MODIS/Terra Snow Cover Monthly L3 Global 0.05Deg CMG, v.6. National Snow and Ice Data Center https://doi.org/10.5067/MODIS/MOD10CM.006 (2015).
83. Kääb, A., Berthier, E., Nuth, C., Gardelle, J. & Arnaud, Y. Contrasting patterns of early twenty-first-century glacier mass change in the Himalayas. *Nature* **488**, 495–498 (2012).
84. Pellicciotti, F., Buergi, C., Immerzeel, W. W., Konz, M. & Shrestha, A. B. Challenges and uncertainties in hydrological modeling of remote Hindu Kush–Karakoram–Himalayan (HKH) basins: suggestions for calibration strategies. *Mt. Res. Dev.* **32**, 39–50 (2012).
85. Nash, J. E. & Sutcliffe, J. V. River flow forecasting through conceptual models part I—a discussion of principles. *J. Hydrol.* **10**, 282–290 (1970).
86. Moriasi, D. N. et al. Model evaluation guidelines for systematic quantification of accuracy in watershed simulations. *Trans. ASABE* **50**, 885–900 (2007).
87. *Food Balance Sheets. A Handbook* (FAO, 2001).

Acknowledgements

Part of this work was carried out by the Himalayan Adaptation, Water and Resilience (HI-AWARE) consortium under the Collaborative Adaptation Research Initiative in Africa and Asia (CARIAA) with financial support from the UK government's Department for International Development and the International Development Research Centre, Ottawa, Canada. Part of this work was performed for the project 'Targeting a climate change hotspot: science to support the SDGs and sustainable water management in the transboundary Indus river basin (SustainIndus)' and received funding from the Netherlands Organization for Scientific Research under the WOTRO Joint Sustainable Development Goals (SDG) research programme (grant W 07.30318.002). The views expressed in this work are those of the creators and do not necessarily represent those of the UK government's Department for International Development, the International Development Research Centre, Canada, or its board of governors and are not necessarily attributable to their organizations.

Author contributions

A.F.L., H.B., C.S. and W.W.I. designed the study. R.R.W., A.F.L. and S.N. developed and ran the upstream model. H.B. developed the downstream model with help from C.S. A.F.L. downscaled future climate forcing, and H.B. and R.R.W. implemented socio-economic scenarios. A.F.L. and H.B. analysed the data and prepared the figures. A.F.L. wrote the article with major contributions from all co-authors.

Competing interests

The authors declare no competing interests.

Additional information

Extended data is available for this paper at https://doi.org/10.1038/s41558-022-01355-z.

Supplementary information The online version contains supplementary material available at https://doi.org/10.1038/s41558-022-01355-z.

Correspondence and requests for materials should be addressed to A. F. Lutz.

Peer review information *Nature Climate Change* thanks Yong Nie, Xiaoming Wang and the other, anonymous, reviewer(s) for their contribution to the peer review of this work.

Reprints and permissions information is available at www.nature.com/reprints.

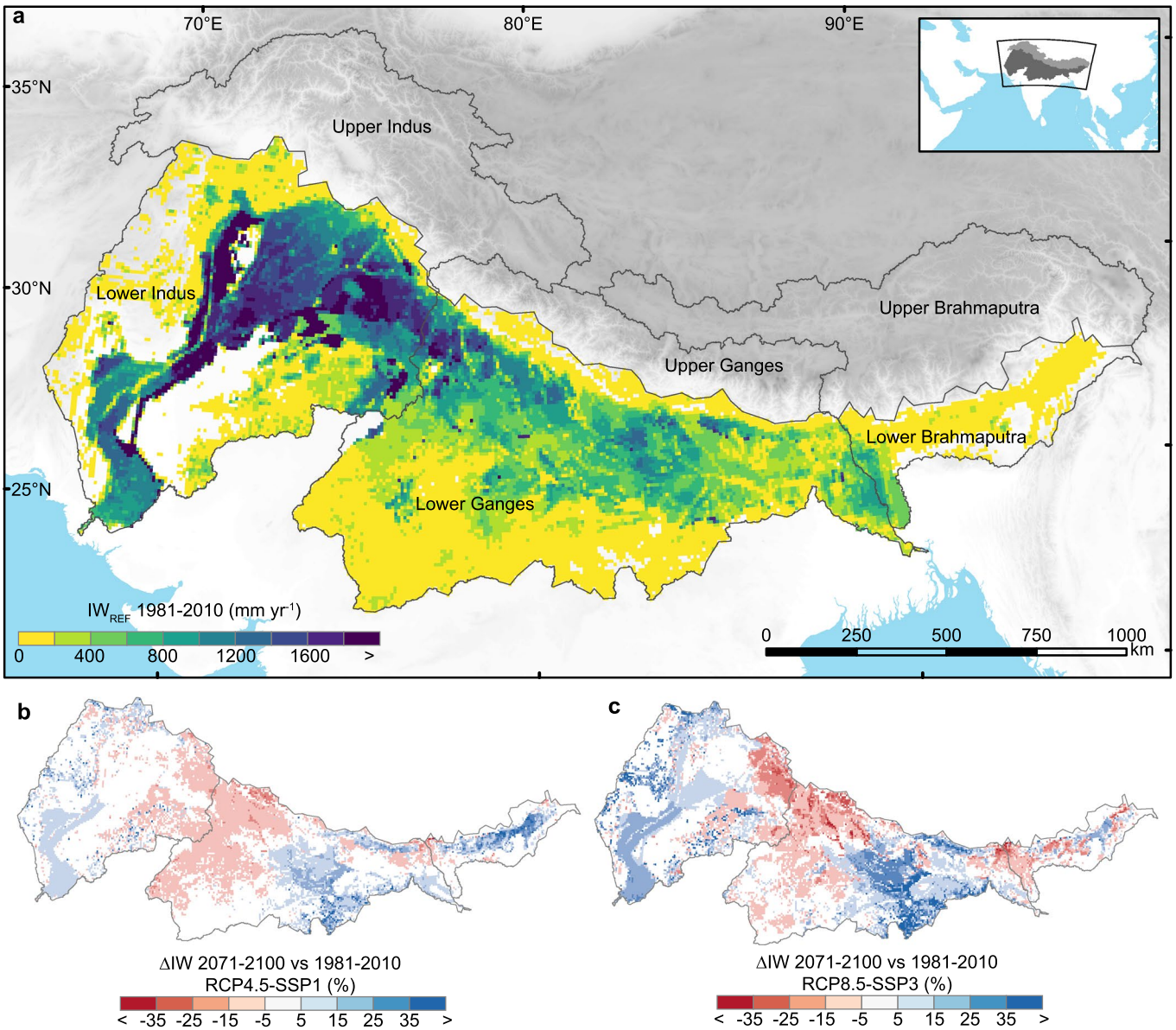

Extended Data Fig. 1 | Historical irrigation withdrawal and projected future changes. Average annual irrigation withdrawals during 1981–2010 (IW_{REF}) (panel **a**). Change in average annual irrigation withdrawal (ΔIW) between 2071–2100 and 1981–2010 for the ensemble mean of RCP4.5-SSP1 (panel **b**) and RCP8.5-SSP3 (panel **c**). Background digital elevation model (GTOPO30) from ref. [45].

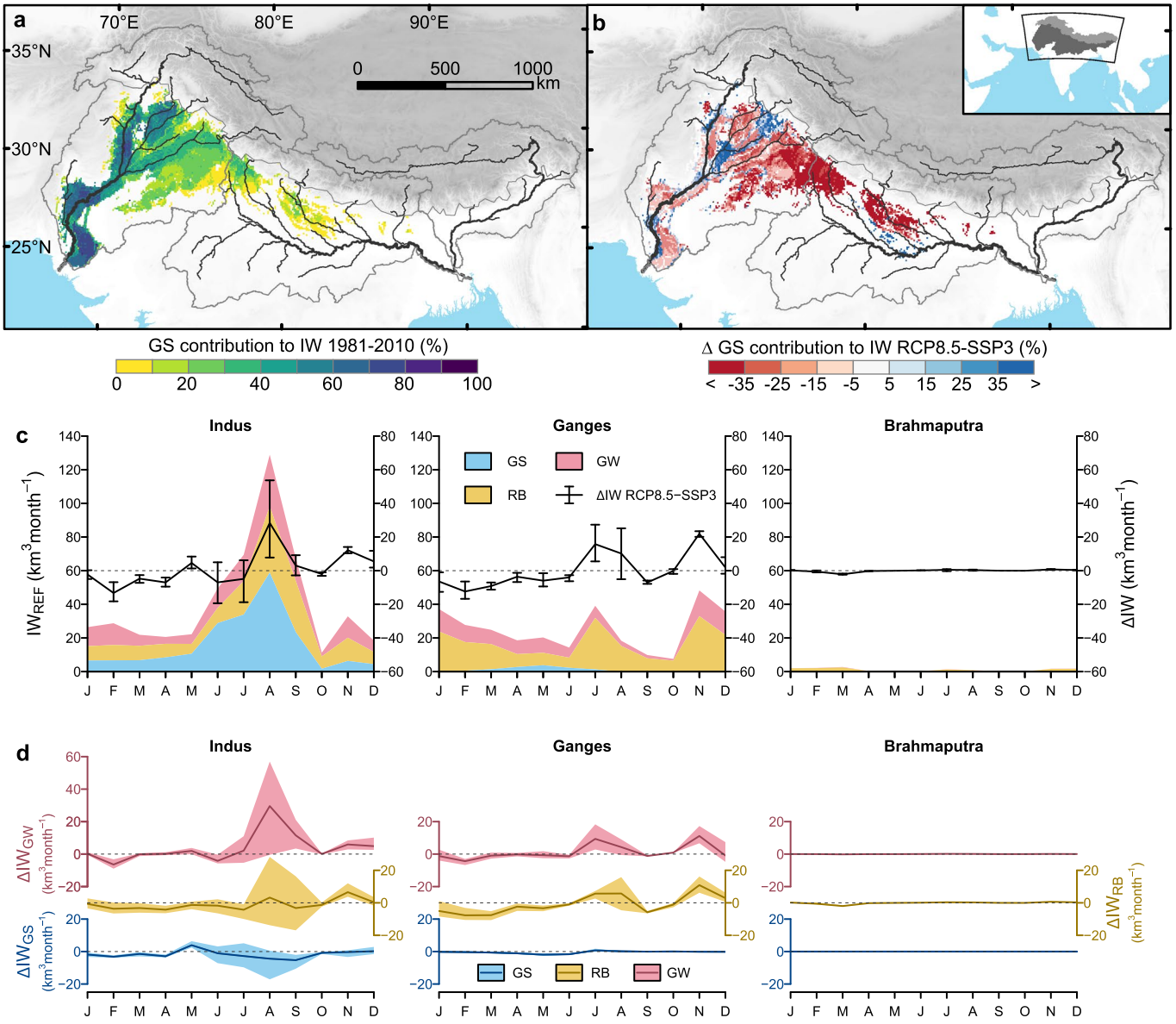

Extended Data Fig. 2 | Historical irrigation withdrawals by source and projected future changes (RCP8.5-SSP3). a) Average contribution of glacier and snowmelt (GS) contribution to irrigation withdrawal during 1981–2010 (IW_{REF}). Grid cells with IW_{REF} < 10 mm yr^{-1} are excluded. **b**) RCP8.5-SSP3 ensemble mean of projected changes in GS contribution to irrigation withdrawal for 2071–2100 vs 1981–2010. **c**) Thirty-year average monthly irrigation withdrawals for the Indus, Ganges and Brahmaputra basins during 1981–2010 differentiated by source. GS = glacier and snowmelt, RB = rainfall-runoff and baseflow, GW = groundwater. Black line indicates RCP8.5-SSP3 ensemble mean of projected change in average monthly total irrigation withdrawal 2071–2100 vs 1981–2010 (ΔIW). Error bars indicate the ensemble spread in projections. **d**) Average monthly projected changes in irrigation withdrawal per source for 2071–2100 vs 1981–2010 (ΔIW). Lines and shading indicate the ensemble mean and ensemble range for RCP8.5-SSP3. Upstream and downstream river basin boundaries (light grey tones) and main rivers (dark grey tones) are indicated in panels a and b. Background digital elevation model (GTOPO30) from ref. [45]. River data from ref. [46].

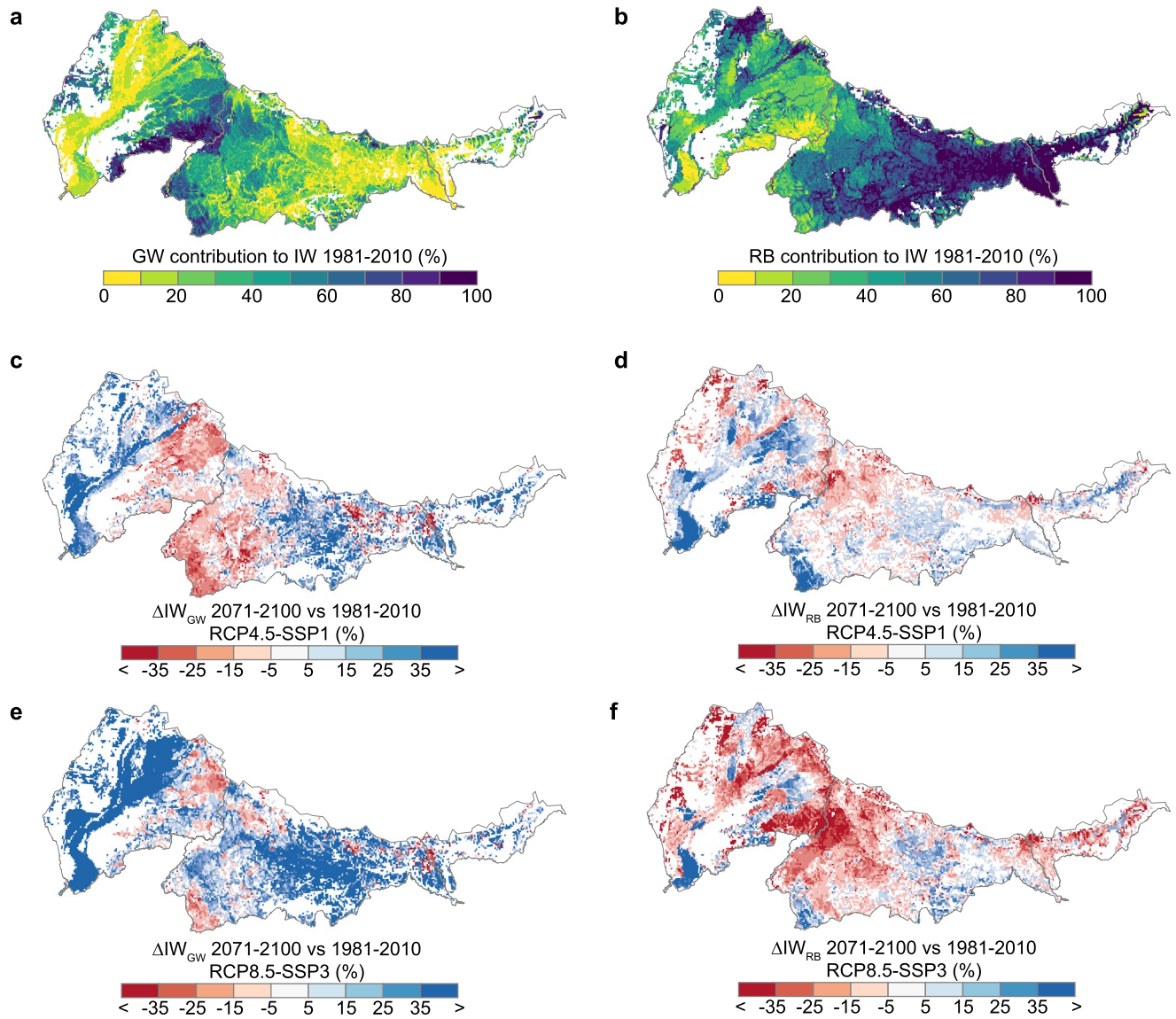

Extended Data Fig. 3 | Historical and projected future contributions to irrigation withdrawals for groundwater and rainfall and baseflow. Contributions of groundwater (GW, panel **a**) and rainfall and baseflow (RB, panel **b**) to irrigation withdrawals (IW) during the reference period. Ensemble mean projections for change in groundwater contribution (ΔIW_{GW}) and rainfall and baseflow contribution (ΔIW_{RB}) between 2071–2100 and 1981–2010 for RCP4.5-SSP1 (panels **c**, **d**) and RCP8.5-SSP3 (panels **e**,**f**).

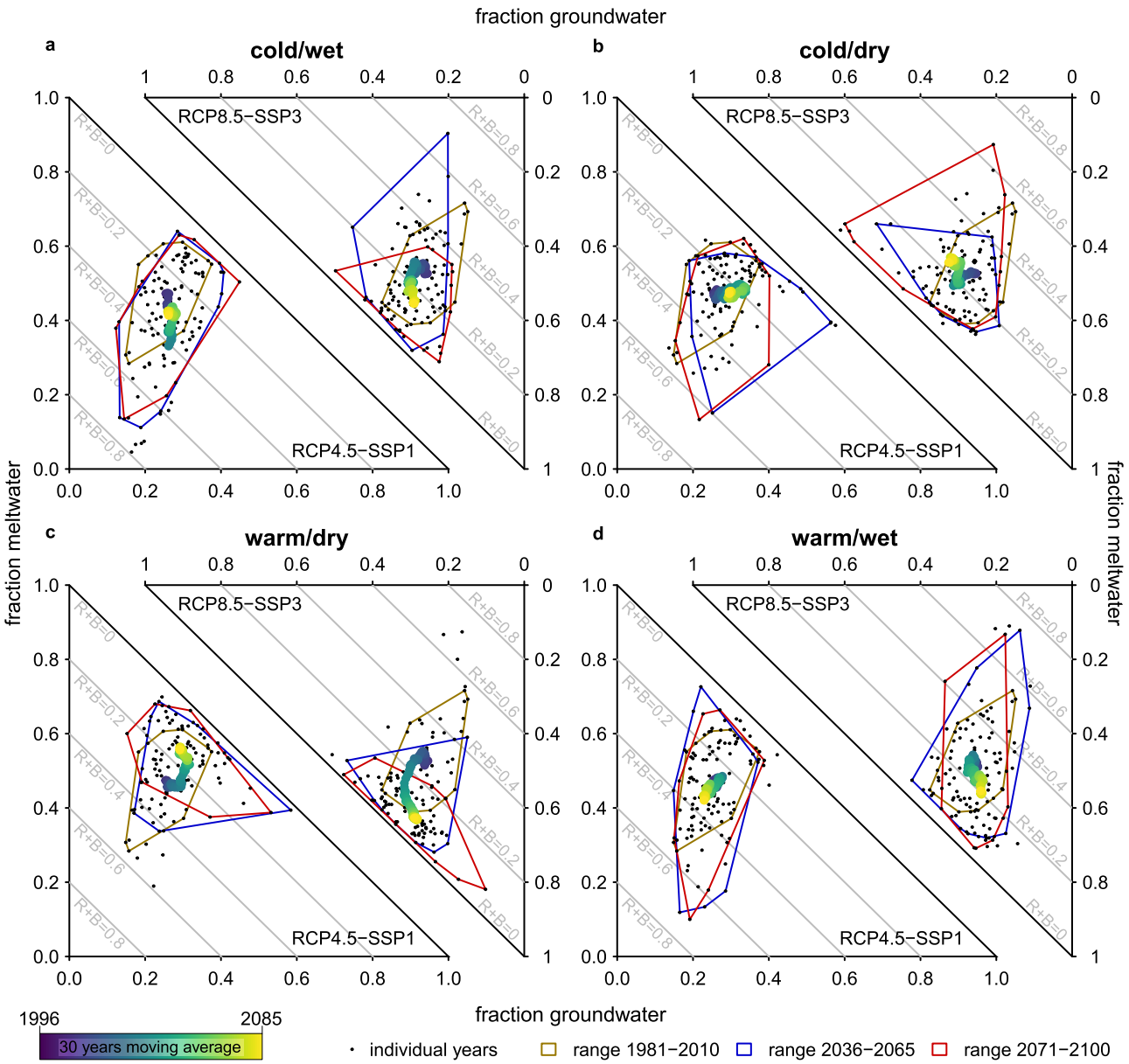

Extended Data Fig. 4 | Shifting sources of irrigation withdrawal in the Indus basin during the month of May. Dots indicate annual fractional basin-averaged contribution to irrigation withdrawal from groundwater (x-axis), meltwater (y-axis) and rainfall and baseflow (indicated by grey lines), for inidvidual years 1981–2100. Convex hulls indicate the range of years 1981–2010, 2036–2065, and 2071–2100). The color scale shows the 30 year moving average starting at 1981–2010 and ending at 2071–2100. Separate plots are shown for cold/wet (**a**), cold/dry (**b**), warm/dry (**c**), and warm/wet (**d**) future scenarios. In each panel results are shown for RCP4.5-SSP1 (lower left part of panel) and RCP8.5-SSP3 (upper right part of panel, with flipped axis direction).

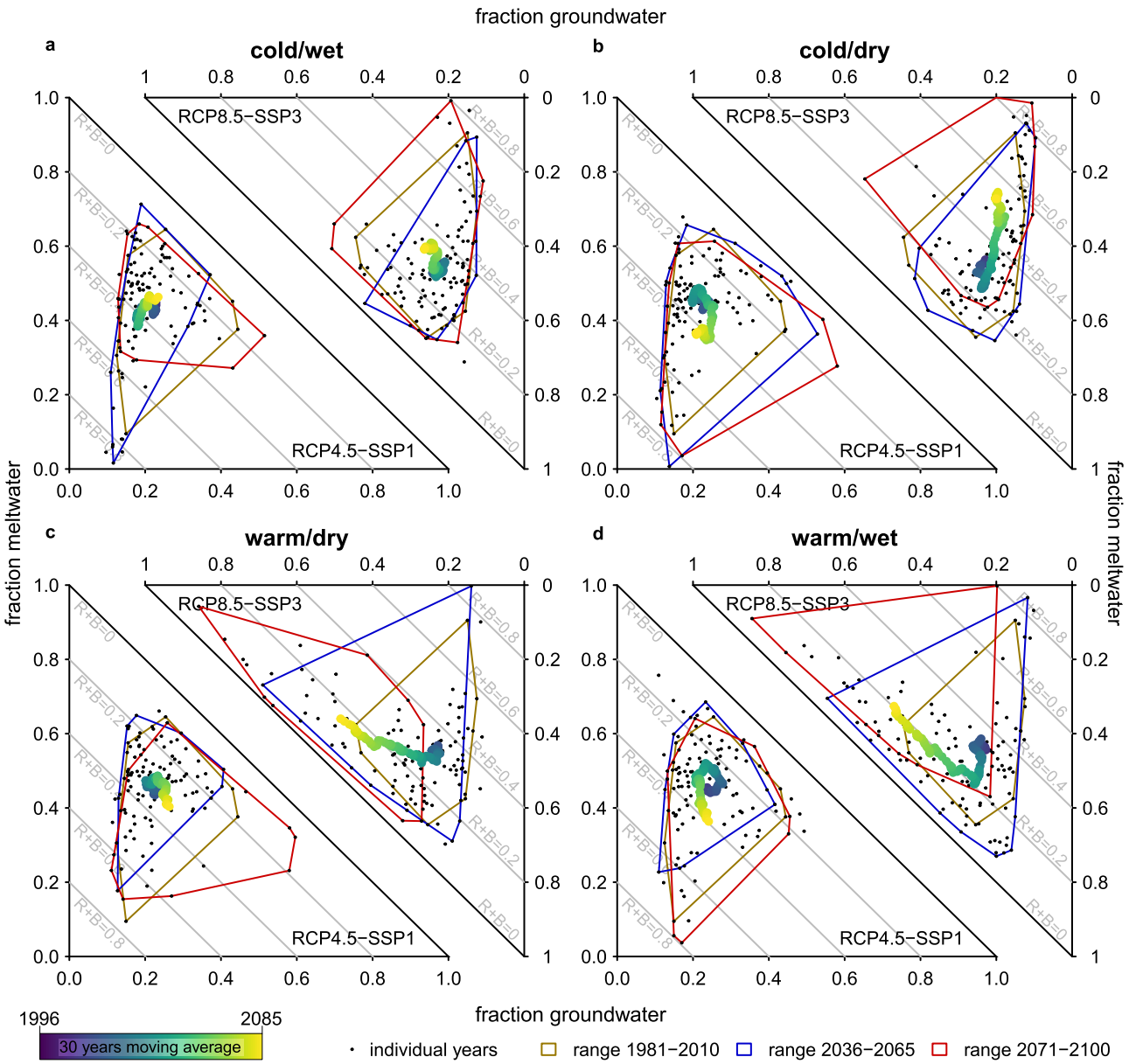

Extended Data Fig. 5 | Shifting sources of irrigation withdrawal in the Indus basin during the month of August. Dots indicate annual fractional basin-averaged contribution to irrigation withdrawal from groundwater (x-axis), meltwater (y-axis) and rainfall and baseflow (indicated by grey lines), for inidvidual years 1981–2100. Convex hulls indicate the range of years 1981–2010, 2036–2065, and 2071–2100). The color scale shows the 30 year moving average starting at 1981–2010 and ending at 2071–2100. Separate plots are shown for cold/wet (**a**), cold/dry (**b**), warm/dry (**c**), and warm/wet (**d**) future scenarios. In each panel results are shown for RCP4.5-SSP1 (lower left part of panel) and RCP8.5-SSP3 (upper right part of panel, with flipped axis direction).

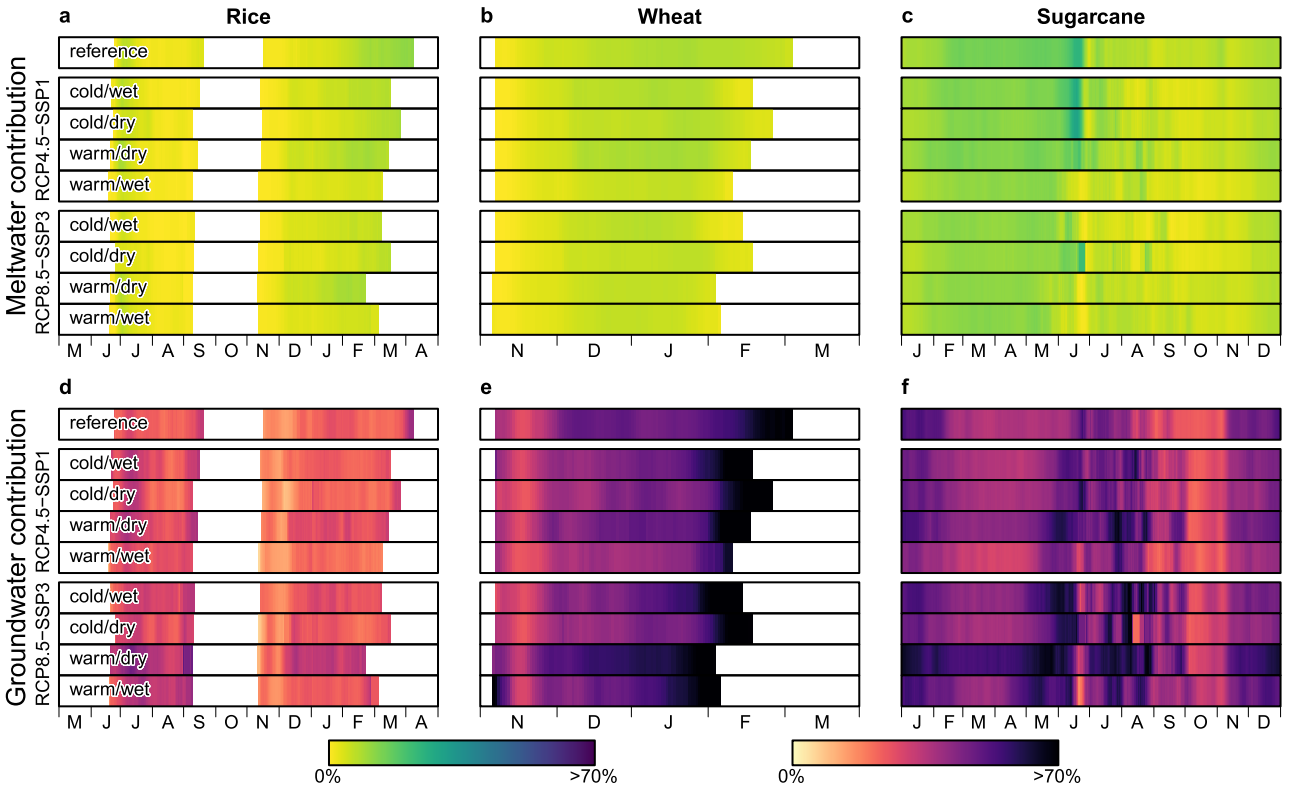

Extended Data Fig. 6 | Contribution of meltwater and groundwater to irrigation for key crop types in the Ganges river basin. Panels a-c show the 30 year daily mean contribution of meltwater to irrigation during the reference period (1981–2010) and end of century period (2071–2010) for each ensemble member in the RCP4.5-SSP1 and RCP8.5-SSP3 ensembles, for rice (**a**), wheat (**b**), and sugarcane (**c**). Panels d-f show the same for the groundwater contribution to irrigation for rice (**d**), wheat (**e**), and sugarcane (**f**).